A&A, 689, A206 (2024)
https://doi.org/10.1051/0004-6361/202450349


Astronomy & Astrophysics

# Detection and characterization of detached tidal dwarf galaxies

Javier Zaragoza-Cardiel[1,⋆], Beverly J. Smith[2,⋆], Mark G. Jones[2], Mark L. Giroux[2], Shawn Toner[2], Jairo A. Alzate[1], David Fernández-Arenas[3], Divakara Mayya[4], Gisela Ortiz-León[4], and Mauricio Portilla[4]

[1] Centro de Estudios de Física del Cosmos de Aragón (CEFCA), Plaza San Juan 1, 44001 Teruel, Spain
[2] East Tennessee State University, Department of Physics and Astronomy, Johnson City, TN 37614, USA
e-mail: smithbj@etsu.edu
[3] Canada-France-Hawaii Telescope, Kamuela, HI 96743, USA
[4] Instituto Nacional de Astrofísica, Óptica y Electrónica, Luis Enrique Erro 1, Tonantzintla 72840, Puebla, Mexico

Received 12 April 2024 / Accepted 6 June 2024

**ABSTRACT**

Tidal interactions between galaxies often give rise to tidal tails, which can harbor concentrations of stars and interstellar gas resembling dwarf galaxies. Some of these tidal dwarf galaxies (TDGs) have the potential to detach from their parent galaxies and become independent entities, but their long-term survival is uncertain. In this study, we conducted a search for detached TDGs associated with a sample of 39 interacting galaxy pairs in the local Universe using infrared, ultraviolet, and optical images. We employed IR colors and UV/optical/IR spectral energy distributions to identify potential interlopers, such as foreground stars or background quasars. Through spectroscopic observations using the Boller and Chivens spectrograph at San Pedro Mártir Observatory, we confirmed that six candidate TDGs are at the same redshift as their putative parent galaxy pairs. We identified and measured emission lines in the optical spectra and calculated nebular oxygen abundances, which range from $\log(O/H) = 8.10 \pm 0.01$ to $8.51 \pm 0.02$. We have serendipitously discovered an additional detached TDG candidate in Arp72 using available spectra from SDSS. Utilizing the photometric data and the CIGALE code for stellar population and dust emission fitting, we derived the stellar masses, stellar population ages, and stellar metallicities for these detached TDGs. Compared to standard mass-metallicity relations for dwarf galaxies, five of the seven candidates have higher than expected metallicities, confirming their tidal origins. One of the seven candidates remains unclear due to large uncertainties in metallicity, and another has stellar and nebular metallicities compatible with those of a preexisting dwarf galaxy. The latter object is relatively compact in the optical relative to its stellar mass, in contrast to the other candidate TDGs, which have large diameters for their stellar masses compared to most dwarf galaxies. The derived stellar population ages range from 100 Myr to 900 Myr, while the inferred stellar masses are between $2 \times 10^6$ $M_\odot$ and $8 \times 10^7$ $M_\odot$. Four of the six TDGs are associated with the gas-rich M51-like pair Arp 72, one TDG is associated with a second M51-like pair Arp 86, and another is associated with Arp 65, an approximately equal mass pair. In spite of the relatively low stellar masses of these TDGs, they have survived for at least 100–900 Myrs, suggesting that they are stable and in dynamical equilibrium. We conclude that encounters with a relatively low-mass companion (1/10th–1/4th of the mass of the primary) can also produce long-lasting TDGs.

**Key words.** galaxies: abundances – galaxies: dwarf – galaxies: evolution – galaxies: interactions

## 1. Introduction

Galaxy interactions can spawn tidal dwarf galaxies (TDGs), concentrations of gas and young stars in tidal features that resemble dwarf galaxies (Duc & Mirabel 1994; Duc et al. 1997; Duc 2012). Unlike most dwarf galaxies, TDGs are expected to lack a massive dark matter component since they are made of material pulled out from the disk (Barnes & Hernquist 1992; Duc et al. 2004; Bournaud & Duc 2006; Wetzstein et al. 2007; Lelli et al. 2015). Thus, TDGs present a unique opportunity to explore the role of dark matter in galaxy dynamics and understand the interplay between baryonic matter and the invisible dark matter component.

However, simulations suggest dark matter may be tidally stripped from dwarf galaxies during interactions with massive companions (Jackson et al. 2021). Therefore, a lack of dark matter may not be a definitive signature of a TDG.

One way to potentially distinguish TDGs from preexisting dwarf galaxies is via their metallicities. TDGs are expected to have higher abundances of heavier elements than other dwarf galaxies of the same mass and optical luminosity if they were formed from gas and stars previously located within the disk of a more massive galaxy. Hence, comparison to mass-metallicity and luminosity-metallicity relations for normal dwarf galaxies has traditionally been used to identify TDGs (Duc et al. 2000; Weilbacher & Duc 2003; Croxall et al. 2009; Duc 2012; Sweet et al. 2014). However, TDGs formed early in the history of the Universe may have low metallicities similar to other dwarfs (Hunter et al. 2000; Recchi et al. 2015), though this has been questioned (Dumont & Martel 2021). Also, TDGs formed from metal-poor gas from the outskirts of galaxies have a low metallicity (Hunter et al. 2000).

Sometimes TDGs can be misidentified as dark galaxies (Román et al. 2021), which are predicted to be composed of mostly dark matter and devoid of significant stellar populations due to the lack of star formation in low-mass halos and at low metallicity (Gnedin & Kravtsov 2010). Distinguishing between TDGs and dark galaxies requires careful investigation of the dynamics, stellar populations, environment, and history of a system (Cannon et al. 2015; Román et al. 2021; Montes et al. 2024; Du et al. 2024).

⋆ Corresponding authors; jzaragoza@cefca.es, smithbj@etsu.edu

Some TDGs can detach from their parent galaxies and become independent dwarf galaxies (Zwicky 1956), but how frequently this actually happens is a matter of debate. Some estimates suggest that the majority of currently observed dwarf galaxies may have been tidally formed rather than being primordial (Hunsberger et al. 1996; Okazaki & Taniguchi 2000; Dabringhausen & Kroupa 2013). Other calculations indicate that ≤10% of local dwarfs originated as TDGs (Bournaud & Duc 2006; Bournaud 2010; Wen et al. 2012; Kaviraj et al. 2012). The reason for the difference of opinion is that the TDG formation rate and survival timescale are not well determined. It has been suggested that many of the dwarf galaxies in the Local Group were formed tidally (Lynden-Bell 1976; Metz & Kroupa 2007; Pawlowski et al. 2012; Fouquet et al. 2012; Hammer et al. 2013; Yang et al. 2014; Pawlowski 2018); however, this idea has been questioned (Duc et al. 2014; Collins et al. 2015; Cautun et al. 2015; Samuel et al. 2021; Sawala et al. 2023; Pham et al. 2023).

Factors that affect the longevity of TDGs include mass loss due to stellar winds and supernovae (Ferrara & Tolstoy 2000; Recchi & Hensler 2007, 2013; Ploeckinger et al. 2015); tidal disruption and compression (Bournaud & Duc 2006; Ploeckinger et al. 2015); and infall back into the parent galaxy (Bournaud & Duc 2006; Hancock et al. 2009). If the star formation rate (SFR) in the TDG is high, stellar feedback may eject much of the gas from the TDG, hastening its demise. Ram pressure stripping by intracluster or intragroup gas or hot halo gas may also affect the evolution of a TDG (Smith et al. 2013). Detailed hydrodynamical simulations (Bournaud & Duc 2006) indicate that more massive objects are more likely to survive, particularly TDGs on low eccentricity orbits formed near the ends of tidal tails and objects produced by approximately equal-mass galaxy pairs. The size and density of satellite dwarfs also affects survival rates (Casas et al. 2012). Interactions and mergers of gas-rich galaxies, such as those at high redshift, produce more TDGs on average (Bournaud et al. 2011; Fouquet et al. 2012).

Even if TDGs do not survive as independent galaxies, their temporary existence may affect the evolution of their parent galaxy and its environment. Star formation and feedback in TDGs may enrich halo gas as well as the intergalactic medium (Duc et al. 2014). Dispersion of the star clusters and individual stars in TDGs and tidal features may contribute to the intragroup, intercluster, and galactic halo globular clusters and diffuse starlight (Mihos et al. 2005). Further, the infall of tidal debris back onto a parent disk (Hibbard & Mihos 1995) may help build the bulge or trigger star formation in the disk.

To better understand the contributions of TDGs to galaxy evolution, it is necessary to look for those that are the most evolved. One way to approach this is to look for detached TDGs, objects that are no longer connected to their parent galaxies by tidal structures.

To this end, we have conducted a systematic multi-wavelength search for detached TDGs in the vicinity of a well-defined sample of nearby interacting galaxies. In this study, we have searched for possible star-forming TDGs outside of optically bright tidal features. We confirmed the redshift coincidence of six candidates via spectroscopic observations. We derived ages, metallicities, and stellar masses for these sources in order to constrain the timescale of formation and their evolutionary history, which we have compared with theoretical models of TDG formation and evolution.

In Section 2, we describe our sample of interacting galaxy pairs and the available imaging data. In Section 3, we explain how we selected candidate TDGs; determined their fluxes in UV, optical, and IR bands; and removed possible interlopers. We present the optical spectroscopy observations and show how we obtained redshifts in Section 4. In Section 5, we provide detailed descriptions of the systems with spectroscopically confirmed TDGs, and we present the analysis of the combined datasets in Section 6. In Section 7, we present the results and compare them to dwarf galaxy relations. We present a discussion of the results and compare with other TDGs in Section 8. Conclusions are given in Section 9.

## 2. Galaxy samples and data

### 2.1. Samples

We started our search for TDGs with the 46 nearby (<150 Mpc) strongly interacting pre-merger pairs of galaxies chosen from the Arp Atlas, the "Spirals, Bridges, and Tails" (SB&T) sample (Smith et al. 2007, 2010, 2016; Smith & Struck 2010; Zaragoza-Cardiel et al. 2018). This sample was previously used to compare the global SFRs and specific SFRs (SFR/stellar mass) of interacting versus spiral galaxies using IR and UV photometry (Smith et al. 2007, 2010; Smith & Struck 2010; Zaragoza-Cardiel et al. 2018). The properties of individual star-forming regions within the disks and tidal features were studied by Smith et al. (2016) and Zaragoza-Cardiel et al. (2018). In the current study, we search for detached TDG candidates outside of optically bright tidal features.

To improve the reliability of our search for TDGs, to be included in our final list of TDG candidates, we required objects to be detected in both the near-ultraviolet (NUV) and at 8 μm (see Section 3.1). Furthermore, since we used *Spitzer* infrared colors to eliminate foreground stars and background quasars from our sample (see Section 3.3), we required the field to be imaged by *Spitzer* in the 3.6 μm and 4.5 μm filters as well. This decreased our initial sample to the 40 interacting pairs that have 3.6 μm, 4.5 μm, and 8 μm and NUV images available. Closer inspection of the available images showed that one of the remaining SB&T galaxies has a field of view of little use around the galaxies. This system was therefore removed from the sample, leaving a final sample of 39 SB&T pairs. These galaxies have a median distance of 44 Mpc.

These interacting galaxies are more nearby than many used in previous searches for TDGs. For comparison, the SDSS-selected TDGs studied by Kaviraj et al. (2012) have a median distance of 226 Mpc, the Hunsberger et al. (1996) TDGs in compact groups have a median distance of 92 Mpc, and the (ultra) luminous infrared galaxies (U/LIRGs) searched by Miralles-Caballero et al. (2012) for TDGs have a median distance of 159 Mpc. Our galaxies are also closer than the compact groups surveyed by Eigenthaler et al. (2015) for TDGs, which have a typical distance of 123 Mpc. This means that our survey will be more sensitive to lower mass objects. However, our galaxies are more distant on average than the TDGs studied in the spectroscopy survey of Duc et al. (2014), which are all closer than 40 Mpc. Our galaxies are also more distant on average than the merger remnants surveyed for dwarf companions by Delgado-Donate et al. (2003), which have a median distance of about 36 Mpc.

Most previous surveys of TDGs focused on objects still embedded in the optically bright tidal structures of interacting galaxies (e.g., Duc & Mirabel 1994; Duc et al. 1997; Smith et al. 2010), while in the current study we searched for star-forming objects outside of classical tidal features. Another difference from earlier surveys is that our systems are relatively isolated

pre-merger pairs, in contrast to TDGs in compact groups (Hunsberger et al. 1996; Eigenthaler et al. 2015), TDGs associated with post-merger early-type galaxies (Duc et al. 2014), or merger remnants and late-stage mergers (Delgado-Donate et al. 2003). In the current study, we focus on the evolutionary stage between tidal tail formation and final galaxian merger. Understanding the dynamical history of these systems will be easier than for later-stage mergers or compact groups. Since our sample is optically selected, the galaxies are less biased toward extreme starbursts than the LIRG/ULIRG systems studied by Miralles-Caballero et al. (2012).

### 2.2. Imaging data

Most of the SB&T systems have been observed in the IR at 3.6, 4.5, 5.8, 8.0, and 24 μm by the *Spitzer* telescope, and in the far-UV (FUV) and near-UV (NUV) filters by the Galaxy Evolution Explorer (GALEX) satellite (Smith et al. 2007, 2010, 2016). In the current study, we only used GALEX images with exposure times greater than 1000 seconds. Many of the SB&T galaxies also have Sloan Digitized Sky Survey (SDSS) optical *ugriz* images available (Smith et al. 2010, 2016). For systems without SDSS images, we use Dark Energy Spectroscopic Instrument Legacy Imaging Surveys (DESI-LIS) *grz* images when available (Dey et al. 2019). About half of the SB&T galaxies have narrowband H$\alpha$ maps available (Smith et al. 2016). About one third have been mapped in the 21 cm HI line. We also used Two Micron All-Sky Survey (2MASS) *J*, *H*, and *K* images[1] to obtain near-IR photometry of our candidate TDGs.

## 3. Candidate tidal dwarf galaxies

### 3.1. Selection of candidate tidal dwarf galaxies

In an earlier study of the SB&T interacting sample (Smith et al. 2016), we searched for TDGs and knots of star formation associated with tidal structures brighter than an SDSS *g* band surface brightness $\mu_g$ of 24.58 mag arcsec$^{-2}$ (equivalent to a *B* band surface brightness $\mu_B = 25$ mag arcsec$^{-2}$). When SDSS images were not available, we use an NUV surface brightness of 26.99 mag arcsec$^{-2}$, which is the equivalent surface brightness assuming a typical NUV − *g* color for tidal tails (Smith et al. 2016).

We now extend that procedure to star-forming regions outside of those limiting isophotes. In this study, we define a "detached TDG" as a TDG that is not connected to the parent galaxy by an optical bridge brighter than $\mu_g = 24.58$ mag arcsec$^{-2}$. These may be TDGs that have already detached from their parent tidal tail or bridge, or whose host tidal structure has stretched or dispersed sufficiently to produce lower surface brightnesses. Our definition of a detached TDG is strictly an operational definition, based on observed optical surface brightness, and is independent of whether or not the TDG is gravitationally bound to the parent galaxy. These candidate detached TDGs may have formed during the current interaction, or they may have been produced during an earlier close encounter between the galaxies in the pair. In some cases, two galaxies in a pair may undergo multiple close encounters before a final merger (e.g., Hancock et al. 2007; Dobbs et al. 2010). Thus more than one generation of TDGs may be produced.

We use the *Spitzer* 8 μm images to identify knots of star formation that lie outside of the SDSS *g* band 24.58 mag arcsec$^{-2}$ isophote or its equivalent. Since the field of view of the GALEX images is large (1.2 degrees diameter), the primary factor that limits how far from the galaxy we can search is the *Spitzer* 8 μm field of view, which is ≥5′ for these galaxies, corresponding to galactic radii of 55 kpc–200 kpc. Computer simulations of TDG formation indicate that the majority of TDGs are found within this distance of the progenitor (Bournaud & Duc 2006).

Our 8 μm plus NUV selection criteria biases the sample toward regions that have formed stars in the last 100 Myr (e.g., Kennicutt & Evans 2012). Thus, we may miss older sources without at least a subset of relatively young stars. However, detection in both of these bands will improve reliability, better ensuring that the sources are star-forming regions rather than foreground stars or background quasars (see Section 3.3). These objects may be knots of star formation that originated in the galaxies and then detached, or dense clumps of gas in extended gas-rich tidal features that have gravitationally collapsed and formed stars.

The TDG selection process was done automatically, searching the 8 μm maps for star-forming regions on two different spatial scales, 1 kpc and 2.5 kpc. Knots of star formation within galaxy disks and tidal features are typically of this size (Smith et al. 2005, 2008; Hancock et al. 2007, 2009), and previously identified TDGs have radii of ∼1–2 kpc (Miralles-Caballero et al. 2012; Duc et al. 2014).

To find candidate TDGs, we smoothed each *Spitzer* 8 μm image to a full width at half maximum (FWHM) resolution of 2.5 kpc, based on the distance to the galaxy. We then used the IRAF[2] routine *daofind* to search for sources on the smoothed image on this scale. With *daofind*, we used a detection threshold of 10$\sigma$ above the noise level in the smoothed images. For the 30 galaxy pairs closer than 67 Mpc, we repeated this process using a FWHM of 1.0 kpc to search for objects on a smaller spatial scale. The 67 Mpc distance limit is set by the spatial resolution of the GALEX and *Spitzer* 24 μm, which limits reliable aperture photometry on smaller scales for more distant galaxies (see Smith et al. 2016).

The edges of many of the *Spitzer* 8 μm images have poorer sensitivity due to decreased coverage during mapping observations. This means that the *daofind* results will be less reliable in these regions. To eliminate these portions of the sky, we used the *Spitzer* 8 μm coverage maps to mask the parts of the images that have *Spitzer* coverages less than 65% of values in the inner regions of the galaxies. To further avoid edge effects we conservatively expanded the mask to include the portions of the images just inside this 65% coverage level, within one resolution element on the smoothed image (i.e., within 2.5 kpc or 1.0 kpc). Since we search for possible foreground or background objects based on the *Spitzer* [3.6]–[4.5] and [3.6]–[8.0] colors (see Section 3.3), we also mask portions of the sky with less than 65% coverage in the 3.6 μm and 4.5 μm bands. Also, since we use detection in the NUV as an additional criteria, we mask areas that are not covered in the NUV image. For a few of the galaxies in our sample, very large field of view *Spitzer* images are available. For these systems, we masked all portions of the images at distances greater than 1 Mpc from both galactic nuclei. All candidate sources found in the masked areas were eliminated from

[1] https://www.ipac.caltech.edu/2mass/overview/about2mass.html

[2] Image Reduction and Analysis Facility, distributed by the National Optical Astronomy Observatories, which are operated by the Association of Universities for Research in Astronomy, Inc., under cooperative agreement with the National Science Foundation.

the survey. If there are other known galaxies in the *Spitzer* 8 μm field at a different redshift from the target galaxy, we masked those galaxies in the image.

### 3.2. Photometry of candidate tidal dwarf galaxies

For each candidate TDG, we extracted photometry in all of the available filters using the IRAF *daophot* command. The photometry was done on the original unsmoothed images using aperture radii of either 1.0 kpc or 2.5 kpc. We applied aperture corrections to the photometry to account for spillage outside of the aperture due to the point spread function. The aperture corrections were calculated as in Smith et al. (2016) and Zaragoza-Cardiel et al. (2018).

### 3.3. Identifying possible interlopers in the tidal dwarf galaxy sample

Some of the candidate TDGs found by the above procedure may be foreground stars, background quasars, or background galaxies. Before doing follow-up spectroscopic observations to confirm redshifts, we first searched the NASA Extragalactic Database[3] (NED) for published redshifts of the objects, and eliminated known background objects.

In the absence of published redshift measurements, some interlopers can be tentatively identified using their *Spitzer* IR colors. As noted in Smith et al. (2016), sources with [3.6]–[8.0] < 0.6 and −0.3 < [3.6]–[4.5] < 0.3 may be foreground stars because in the 3.6–8 μm range stars spectral energy distributions (SEDs) drop so [3.6]–[4.5] and [3.6]–[8.0] colors are near zero (Whitney et al. 2004) . Sources with [3.6]–[4.5] > 0.3 and 1.0 < [3.6]–[8.0] < 3.6 could be background active galactic nucleus (AGN) because they are flat between 3.6–4.5 μm range (Hatziminaoglou et al. 2005) in contrast with the drop in this range of star-forming regions (Smith et al. 2005, 2008, 2014), so background AGNs have redder [3.6]–[4.5] colors. Star-forming regions with metallicities larger than that of the Small Magellanic Cloud (SMC) ($12 + \log\frac{O}{H} = 8.03$, Russell & Dopita 1992) are unlikely to fall in these ranges (Smith et al. 2016). Since TDGs are more metal rich than common dwarf galaxies we probably do not lose TDGs using these color criteria.

It is possible that low metallicity dwarf galaxies may fall in these regions in color-color plots, since galaxies with low metallicities are often faint in the polycyclic aromatic hydrocarbon (PAH) features that contribute to the *Spitzer* 8 μm band (Houck et al. 2004; Madden et al. 2006; Hunt et al. 2010). This means that low metallicity objects may have bluer [3.6]–[8.0] colors than higher metallicity galaxies (Rosenberg et al. 2008). Furthermore, low metallicity systems may have redder [3.6]–[4.5] colors than solar-metallicity galaxies (Smith & Hancock 2009).

However, as noted above, true TDGs are expected to have higher metallicities than classical dwarfs and are thus expected to have *Spitzer* colors similar to those of star-forming regions within galaxy disks. We therefore eliminated candidates outside of the IR color ranges given above as likely background or foreground objects.

We also used published redshifted narrowband H$\alpha$ images of the systems (references tabulated in Smith et al. 2016) to search for possible H$\alpha$ detections of the candidate TDGs. A reliable detection of a candidate TDG means that it is likely at the same redshift as the parent galaxy. However, artifacts in the H$\alpha$ maps due to imperfect continuum subtraction because of mis-matches in the point spread function of the on-line and off-line images may lead to false detections at low S/N. Thus tentative detections of H$\alpha$ from these images must be confirmed with follow-up spectroscopy.

We also searched the literature for 21 cm HI maps of the systems, and prioritized candidate TDGs that lie within or near HI concentrations at the same redshift as the galaxy pair. Positional coincidence of a UV/optical/IR source with such an HI cloud is strong evidence that it may be associated with the galaxy pair. However, it is possible that the UV/optical/IR source is merely a background object behind the HI cloud, and thus the redshift must be confirmed via optical spectroscopy.

## 4. Longslit spectra observations

Based on the above selection criteria, including the presence of H$\alpha$ and/or HI, we conducted an observational campaign to obtain optical spectra of the most promising TDG candidates. A total of 11 candidate detached TDG were observed; of these, six were found to have redshifts that matched the target galaxy pair, while five were found to have redshifts that did not match the target galaxy pair.

The observations were carried out using the Boller & Chivens spectrograph mounted on the 2.1m telescope at the San Pedro Mártir Observatory. We utilized the 600l/mm grating with a slit width of 3arcsec, providing a spectral resolution of approximately ∼4 Å over a range spanning from 4800 to 7100 Å. A summary of the observations is presented in Table 1. During each night of observations, a spectrophotometric standard star was observed to enable flux calibration of the 1D spectrum. The standard longslit spectral reduction techniques were applied to the data, including cosmic ray removal, bias subtraction, flat field correction, combination of multiple exposures, wavelength calibration, 1D spectra extraction, and sky subtraction. IRAF was used for these tasks.

We found redshifts consistent with those of the possible host systems for six of the candidate TDGs (Table 1). Three of these sources are associated with Arp 72, two with Arp 86, and one with Arp 65. Figure 1 displays DESI-LIS color images of these three systems. The positions of the observed slits are overlaid on the images.

Figure 2 showcases the reduced spectra of these six objects. Emission lines are clearly detected in all objects. In this figure, we provide the redshift estimations based on the H$\alpha$ line and compare them with the values for the parent galaxies reported in NASA NED. The observed redshifts indicate that these TDGs are associated with the interacting pair of galaxies, as the observed velocities are within a difference of 200 km/s or less.

On the other hand, we found that five of the detached TDG candidates are not at the redshift of their supposed parent galaxy (see Table 1). So, we confirm that these five objects are not detached TDGs, but background galaxies. We show the observed spectra of these five objects in Fig. 3, where the redshifted H$\beta$ and [O III]$\lambda$4959+$\lambda$5007 emission lines are clearly seen. The measured redshift for each TDG candidate is shown in Fig. 3 together with the redshift of the supposed parent galaxy. The reason they have been observed just once ($N_{obs}$) is because we could clearly see the emission lines immediately after the observation, so we decided to not continue the observation of these objects. The exception is Arp244a, since those observations were performed on service mode and we could not make decisions in real time.

[3] http://ned.ipac.caltech.edu

**Table 1.** Observing log and derived redshifts.

| ID | RA deg | Dec deg | Date mm/dd/yyyy | $t_{exp}$ min | $N_{obs}$ | Spectral range Å | $z$ |
|---|---|---|---|---|---|---|---|
| Arp65a | 5.4882353 | 22.3789987 | 10/30/2022 | 90 | 4 | [4780–7100] | $0.0185 \pm 0.0003$ [(a)] |
| Arp72a | 236.7662451 | 17.8746735 | 05/04/2022 | 60 | 5 | [4780–7100] | $0.00113 \pm 0.0003$ [(a)] |
| Arp72b | 236.7195719 | 17.8894956 | 05/03/2022 | 60 | 5 | [4500–6820] | $0.0106 \pm 0.0003$ [(a)] |
| Arp72c | 236.7073667 | 17.8718278 | 05/05/2022 | 60 | 5 | [4780–7100] | $0.0111 \pm 0.0003$ [(a)] |
| Arp86a | 356.78143 | 29.448372 | 10/28/2022 | 60 | 3 | [4780–7100] | $0.0164 \pm 0.0003$ [(a)] |
| Arp86b | 356.76018 | 29.462161 | 10/29/2022 | 60 | 1 | [4780–7100] | $0.2482 \pm 0.0004$ [(b)] |
| Arp86d | 356.77929 | 29.467247 | 10/28/2022 | 60 | 3 | [4780–7100] | $0.0167 \pm 0.0003$ [(a)] |
| Arp86e | 356.74349 | 29.439117 | 10/29/2022 | 60 | 1 | [4780–7100] | $0.1158 \pm 0.0004$ [(b)] |
| Arp87b | 175.17772 | 22.462017 | 5/04/2022 | 60 | 1 | [4780–7100] | $0.1119 \pm 0.0004$ [(b)] |
| Arp244a | 180.54481 | −18.910464 | 01/31/2022 | 60 | 2 | [4660–6980] | $0.1508 \pm 0.0004$ [(b)] |
| Arp256a | 4.6977042 | −10.36316 | 10/28/2022 | 45 | 1 | [4780–7100] | $0.1011 \pm 0.0004$ [(b)] |

**Notes.** [(a)]Association with Parent Galaxies Confirmed by Redshift. [(b)]Confirmed Background Object.

Serendipitously, we found a detached TDG candidate near the Arp72 system in the DESI-LIS color images which is at the same redshift of Arp72. This source is hereafter identified as Arp72d. This TDG candidate was not in our list of candidates because it is not covered by *Spitzer* 8 µm band observations. We show the Arp72d TDG candidate in Fig. 4 together with the SDSS optical spectra of the object taken from SDSS-DR16 (Ahumada et al. 2020). The observed redshift indicates that this TDG is also associated with the Arp72 system of interacting galaxies.

It is possible that some of the confirmed detached TDGs may actually be preexisting dwarf galaxies rather than TDGs. Metallicity could be used as a potential discriminator in this regard. We have successfully detected multiple emission lines from these objects: H$\beta$, H$\alpha$, [O III]$\lambda$4959+$\lambda$5007, [N II]$\lambda$6548+$\lambda$6583 and [S II]$\lambda$6717+$\lambda$6731. These lines allowed us to estimate the oxygen abundance using the Pilyugin & Grebel (2016) strong line calibrator method (Section 5.1).

The underlying stellar continuum is visible in Arp86a and to a lesser extent in Arp72a. In these two cases, we fitted the stellar continuum to the observed spectra using the Galaxy IFU Spectroscopy Tool (GIST) pipeline (Bittner et al. 2019). The fitting procedure utilized penalised pixel-fitting (pPXF) code (Cappellari 2017) and the Medium resolution INT Library of Empirical Spectra (MILES, Vazdekis et al. 2010) to model the continuum and absorption lines. The fit was performed over the observed spectral range (refer to Table 1) using the spectral resolution measured as the median width of the lines observed in a lamp calibration spectrum, which yielded a FWHM of 4.4 Å.

In this analysis, we focus on the emission lines and the removal of the stellar continuum, without examining the detailed results of the stellar continuum fitting. The primary objective is to recover the fluxes of the emission lines from the observed spectra. To estimate the fluxes from the pure emission line spectra, we employed Specutils[4], an associated package of Astropy (Astropy Collaboration 2022). We utilized derivatives to locate local maxima, while using an emission-free spectral region to estimate the noise level. We considered peaks that were at least six times larger than the noise level as significant. Subsequently, we identified and measured the fluxes of the following lines: H$\beta$, H$\alpha$, [O III]$\lambda$4959+$\lambda$5007, [N II]$\lambda$6548+$\lambda$6583 and [S II]$\lambda$6717+$\lambda$6731 (when detected). The integrated flux was estimated by integrating the flux over the relevant spectral range. To define this range, we identified the upper and lower wavelength limits by calculating the root mean square (rms) of the spectra in a nearby emission-free region and determined the first wavelengths from the maximum flux that crossed the rms. The spectral range used for estimating the integrated flux extended from the lower wavelength crossing the rms, subtracting 4.4 Å, to the upper wavelength crossing the rms, adding 4.4 Å. The spectra were corrected for Galactic extinction before line flux estimation. We also corrected for internal dust extinction using the H$\alpha$-H$\beta$ Balmer decrement, assuming $\frac{I_{H\alpha}}{I_{H\beta}} = 2.863$ (Osterbrock 1989) for case B recombination, and adopting attenuation curve values from Calzetti et al. (2000), with $\kappa_{H\alpha} = 3.33$ and $\kappa_{H\beta} = 4.60$.

Table 2 presents the measured extinction-corrected emission line fluxes for the confirmed detached TDGs, as well as for NGC 5994, the smaller companion of the Arp 72 system, where we utilized the available spectra and emission line fluxes from SDSS centered in NGC5994. Table 2 also provides $E(B-V)$ for each source, as well as our derived values of log(O/H).

To compare the emission line properties of the TDGs with those of the host galaxies (section 6.2), it is necessary for us to obtain optical line fluxes and derive metallicities for star-forming regions within the main disks of the galaxies as well. For Arp 72, we combined the observed spectra with archival data for the main galaxy, NGC 5995, obtained by the Multi Unit Spectroscopic Explorer (MUSE, Bacon et al. 2010). MUSE is an integral field spectrograph installed on the Very Large Telescope (VLT), offering a field of view of $1 \times 1$ arcmin$^2$, a spectral range between 4800 and 9300 Å, and a spectral resolution ranging from 2.4 to 3 Å. The MUSE observation of Arp 72 covers the white square area shown in Figure 1 (middle). We performed stellar continuum subtraction as described earlier, while considering the different spectral resolution of the MUSE data. The stellar continuum was fitted between 4800 and 6850 Å, aligning the minimum spectral resolution of 2.5 Å with that of the MILES library. Subsequently, we estimated the fluxes for the same emission lines as the TDGs, following the same procedure. For Arp 86, we combined our flux measurements with those reported in Zhou et al. (2014). For Arp 65, we used the reported oxygen abundances from Zhou et al. (2014) and Zasov et al. (2020), as they employed the same calibrator we used, the S-calibrator from Pilyugin & Grebel (2016).

[4] https://specutils.readthedocs.io

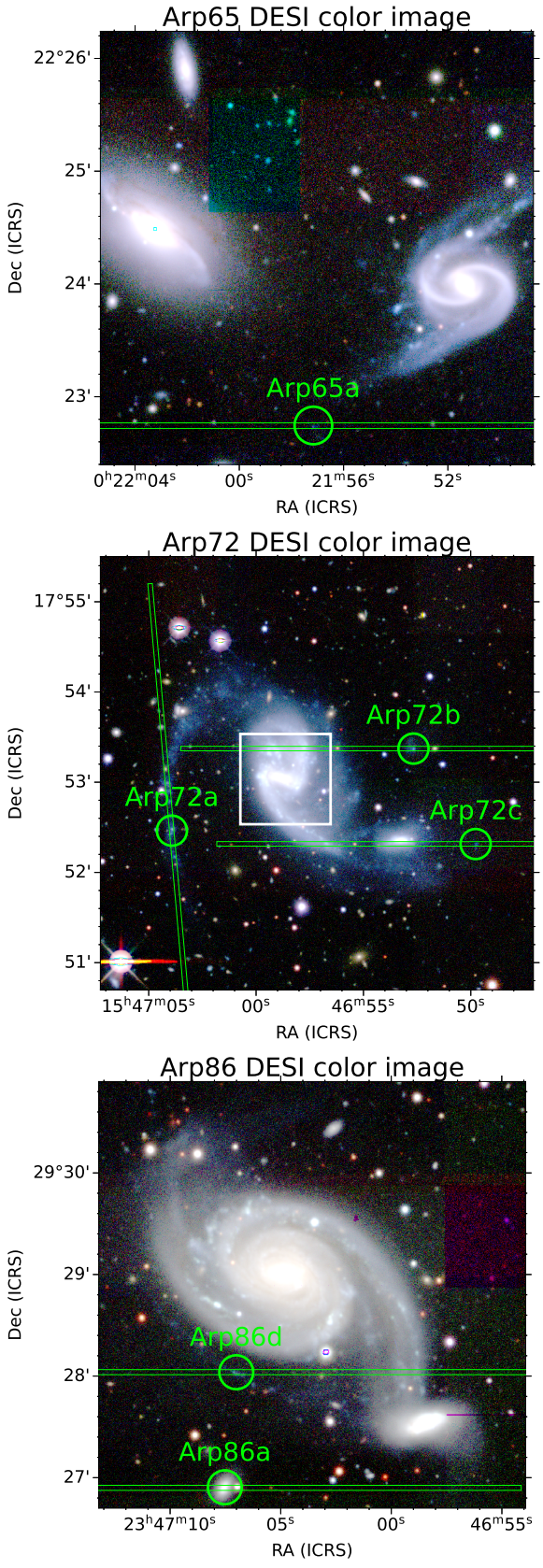


**Fig. 1.** DESI-LIS color image of the galaxies in which we have identified and confirmed detached TDGs. The TDGs are shown as green circles. The slit positions of the spectrograph are shown in green. The MUSE field of view for the primary galaxy in Arp 72, NGC 5996, is marked by a white box in the middle panel. The green square in the top panel is an artifact in the DESI-LIS color map.

We provide the UV/optical/IR photometry of the final sample of redshift-confirmed detached TDGs in Table 3. The fluxes in Table 3 have been corrected for Galactic extinction. In Section 5.2, we use this photometry to compute and fit the SEDs of the TDGs.

## 5. Detailed description of systems

### 5.1. Arp 65

Arp 65 (Figure 1, top panel) consists of two spirals, NGC 90 to the west and NGC 93 to the east. NGC 93 shows two long straight tidal tails extending from a "grand design" two-armed spiral pattern in the inner disk. The edge-on disk galaxy NGC 93 has a 3.5 μm flux three times that of the western galaxy (Smith et al. 2007) and an estimated stellar mass three times larger (Sengupta et al. 2015). A 21 cm HI map of the pair has been presented by Sengupta et al. (2015), who conclude that NGC 93 is gas-poor and NGC 90 gas-rich. Both have peculiar HI morphologies. The HI associated with NGC 93 is skewed to the north relative to the optical galaxy, while a massive concentration of HI ($3.4 \pm 0.4 \times 10^9$ $M_\odot$) is offset to the southeast of NGC 90. Sengupta et al. (2015) conclude that the most likely explanation for the large concentration of gas outside of NGC 90 is that it was tidally stripped from NGC 90 about 100–250 Myr ago by the interaction with NGC 93. Alternatively, Zasov et al. (2020) suggest that this gas was removed by ram pressure stripping due to motion through intragroup gas.

Extra-nuclear knots of star formation are detected near the base of the tidal features of NGC 90 in the UV (Smith et al. 2010; Sengupta et al. 2015) and in optical emission lines including H$\alpha$ (Zasov et al. 2020). Our detached TDG lies further away from NGC 90 than these sources, near the southern end of the HI concentration. Our best-fit determination of the starburst age of this TDG (see Section 6.2), $110 \pm 50$ Myr, is consistent with the Sengupta et al. (2015) interaction age, supporting the idea that this star formation was triggered by the interaction.

### 5.2. Arp 72

The M51-like galaxy Arp 72 (Fig. 1, middle panel) is composed of the larger galaxy NGC 5996 in the east and a small companion NGC 5994 to the west, connected by an optical bridge. The 3.6 μm flux of the primary is 12 times that of the companion (Smith et al. 2007). In UV images, a long (3′; 47 kpc) curved tidal tail extends to the east from the primary galaxy (Smith et al. 2010); this tail is also visible in optical pictures but is not as prominent in the optical as in the UV. The 21 cm HI map of Sengupta et al. (2012) shows that this tail is also rich in HI. Another HI tail extends 1′ (15 kpc) to the west of the companion (Sengupta et al. 2012).

TDG Arp72a is located within the long HI-rich tail to the east, and is clearly tidal in origin. However, the optical surface brightness of the surrounding tail is below our nominal cut-off, and thus by our definition, this TDG is classified as "detached". TDG Arp72b is located near the end of a shorter extension of HI to the northeast, while TDG Arp72c is within the western HI tail. Arp72b and Arp72c are clearly tidal in origin, and are unambiguously "detached" in the sense that they are not connected to the main galaxy by an optically visible tail. However, they are still connected to the main galaxy via gaseous features. Arp72d is located at 5′ (80 kpc) from the main galaxy, NGC5996. Arp72d is not in the field of view of the HI map presented in Sengupta et al. (2012). Within the field of view, no

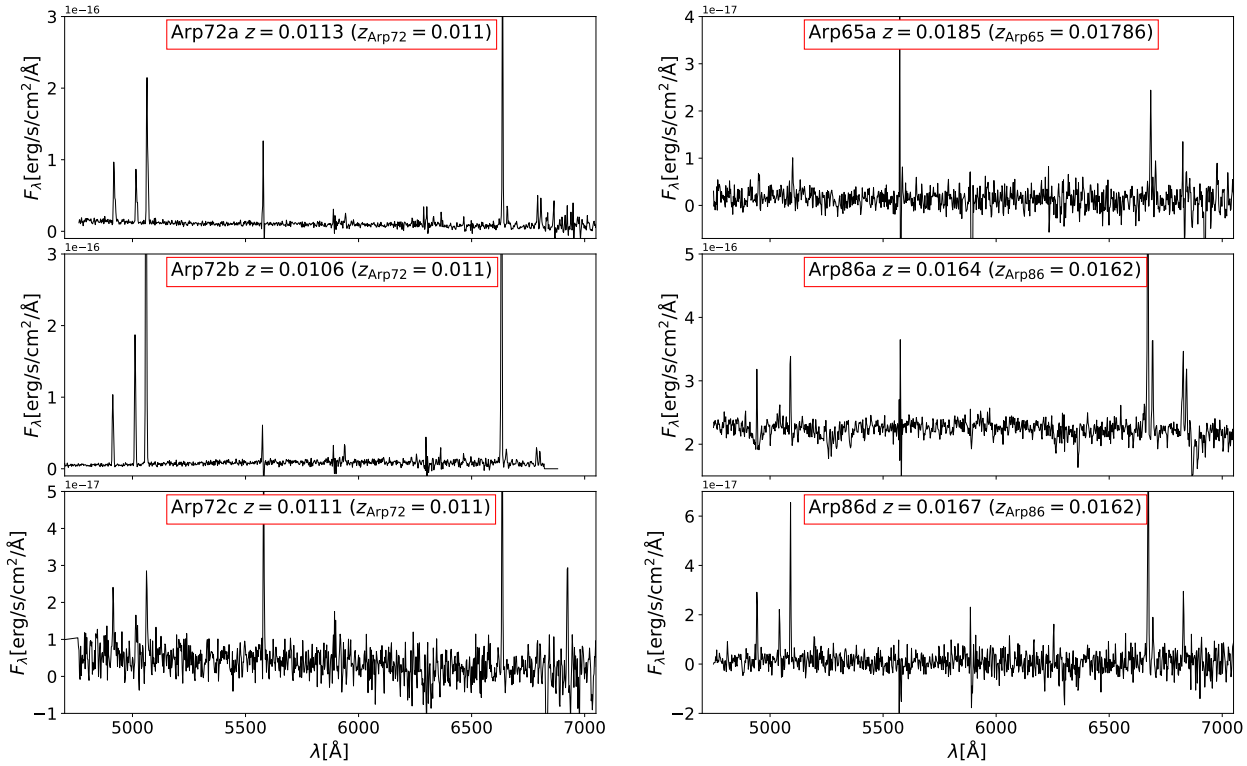


**Fig. 2.** Spectra for the six TDGs confirmed to be at the redshift of the parent galaxies. In the red boxes, redshifts derived from H$\alpha$ are shown and compared with that of the host galaxy.

HI tail connects the main galaxy to the area where Arp72d is located.

Near the position of Arp 72c, the HI velocity field of Sengupta et al. (2012) at 40″ resolution shows a gradient, with positive velocities relative to the systematic velocity to the east of Arp 72c and negative velocities to the west. Over a scale of about 20″ east-west, the radial velocity changes by about 20 km s$^{-1}$. However, this trend may be part of a smooth gradient extending from the eastern side of the companion galaxy NGC 5994, rather than a signature of rotation within the TDG. Higher spatial resolution data is needed to test this.

### 5.3. Arp 86

Arp 86 (Fig. 1, bottom panel) is another M51-like interacting pair. The primary galaxy NGC 7753 in the north has a 3.6 μm flux five times that of the smaller companion NGC 7752 in the south. The HI map of Sengupta et al. (2009) reveals a HI countertail to the north, a tail that is not present in UV or optical maps (Smith et al. 2010). To the southeast of the companion, two parallel HI tails are seen (Sengupta et al. 2009). From H$\alpha$ rotation curves, Marcelin et al. (1987) infer that the ratio of the dynamical masses of the two galaxies in the pair is 1:10.

The candidate TDG we name Arp86a is listed in the 2MASS catalog as 2MASX J23470758+2926531. This object has previously been studied by Zhou et al. (2014), who find a redshift and metallicity consistent with our values. Sengupta et al. (2009) find an HI counterpart to this source, and derive an HI mass of $4.5 \times 10^8$ M$_\odot$. They state that the HI spectrum resembles a weak double horn consistent with rotation, but we note that its spectrum might be affected by tidal features near the galaxy. As noted below (Section 7.1), in metallicity-M* relations, this object lies in the region populated by normal dwarf galaxies; thus, it is likely a preexisting dwarf rather than a true TDG.

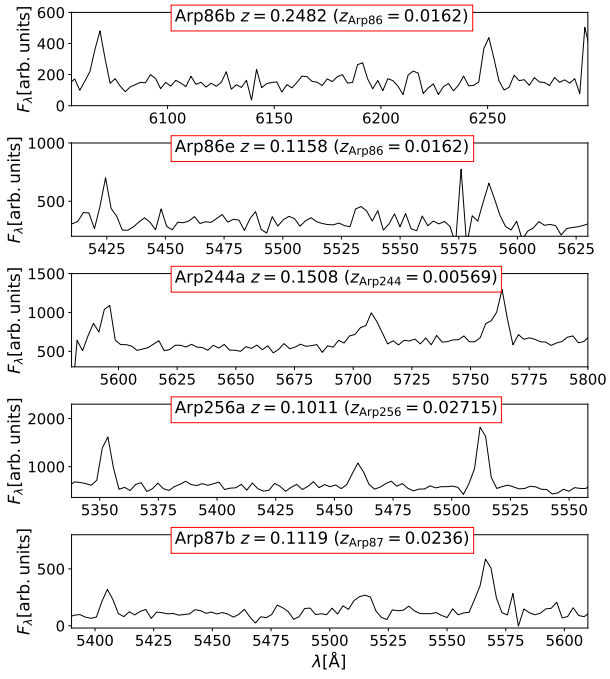


**Fig. 3.** Spectra for the 5 objects confirmed to not be at the redshift of the parent galaxies. In the red boxes, redshifts derived from H$\beta$ are shown and compared with that of the host galaxy.

Confirmed TDG Arp86d is a relatively low stellar mass ($3.6 \pm 1.2 \times 10^6$ $M_\odot$) object (see Section 6.2) just outside of the

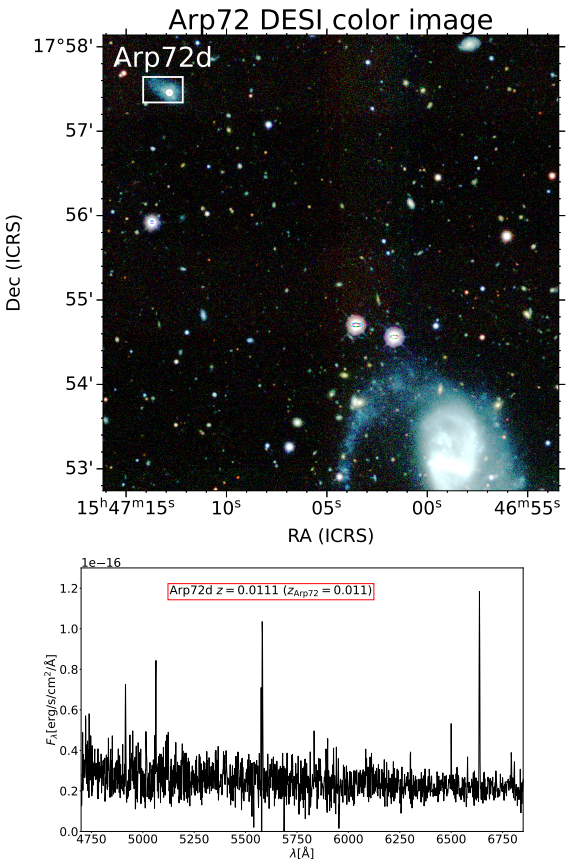


**Fig. 4.** DESI-LIS color image of the Arp72d TDG candidate (top) and its optical spectrum from the SDSS (bottom). The TDG candidate is shown in the white square (northeast of Arp72), while the SDSS fiber where the spectrum is taken is shown as a white circle.

main disk of NGC 7753. It appears to be part of a faint outer spiral arm of this galaxy seen in UV maps (Smith et al. 2010).

We also obtained optical spectra of two other candidate TDGs in the vicinity of Arp 86, but both were found to be background objects (see Table 1).

## 6. Analysis

### 6.1. Oxygen nebular abundance

The discrimination between TDGs and ordinary dwarf galaxies using the nebular oxygen-to-hydrogen (O/H) abundance-stellar mass relation depends on reliably distinguishing low and high oxygen abundances. We used the Pilyugin & Grebel (2016) strong line calibrator, which is capable of doing so. Since the [OIII]4959 and [NII]6548 lines are marginally detected from our sources (if detected), we used the theoretical relation of one-third with respect to their doublet-companion lines, [OIII]5007 and [NII]6583, respectively (Pérez-Montero 2017). The derived oxygen abundances are given in Table 2. We used the same method to obtain abundances for the star-forming regions within the main galaxies of Arp 65 and Arp 72.

### 6.2. Ultraviolet to mid-infrared spectral energy distribution fitting

We have utilized our photometry to perform stellar population and dust emission fitting using the Code Investigating GALaxy Emission (CIGALE, Boquien et al. 2019). The observational data used in the fitting process are listed in Table 3.

For the modeling, we assumed a double exponential star formation history, a modified dust law based on Calzetti et al. (2000) and Leitherer et al. (2002), single stellar populations (SSPs) from Bruzual & Charlot (2003), and the dust emission model proposed by Draine et al. (2014). The allowed parameters for the different models are presented in Table 4. The results obtained from the CIGALE fits are summarized in Table 5, and the observed and fitted SEDs are shown in Figure 5.

## 7. Results

### 7.1. Comparison with standard mass-metallicity relations for dwarf galaxies

The fundamental relation between metallicity and stellar mass could be used as a discriminator between TDGs and preexisting dwarf galaxies. In Figure 6, we plot the stellar metallicity versus stellar mass for the TDGs. We observe a clear division in stellar mass, where a group of six TDGs has stellar masses ($M_*$) less than $1 \times 10^8$ $M_\odot$, and one TDG (Arp86a) stands out as significantly more massive with $M_* = 1.4 \times 10^9$ $M_\odot$. Comparing these results with the relation for dwarf galaxies from Kirby et al. (2013), we see that four sources, Arp 65a, Arp 72c, Arp86d, and Arp72a lie significantly above the standard relation, taking into account the uncertainties in the stellar metallicities obtained from CIGALE. For the remaining TDGs, however, there are large enough uncertainties in the metallicity to make it difficult to discriminate between the two options. It is important to note that the relation from Kirby et al. (2013) uses iron abundances, [Fe/H], rather than direct metallicity values $Z$. However, for a first-order approximation, these values can be considered equivalent.

The nebular oxygen abundance versus stellar mass is plotted in Fig. 7. We overlap on this plot the relations reported by Duarte Puertas et al. (2022) for star-forming SDSS galaxies with $\log(M_*) > 8.5$, which was also derived using the Pilyugin & Grebel (2016) strong-line method. We have also overlayed the Berg et al. (2012) relation for dwarf galaxies. The latter curve was obtained using oxygen abundances derived using the "direct" method of deriving oxygen abundances (i.e., using electron temperatures calculated from the [O III]$\lambda$ 5007/[O III]$\lambda$ 4363 emission line ratio). According to Pilyugin & Grebel (2016), oxygen abundances from their strong-line method agrees with the "direct" method within 0.1 dex. In Fig. 7, the group of less massive TDGs clearly exhibits higher oxygen abundances compared to other dwarf galaxies with similar masses, even when accounting for the additional uncertainty of 0.1 dex due to the different methods of obtaining the oxygen abundances. However, the most massive object, Arp86a, might not be a true TDG since its oxygen abundance is quite close to that expected in the fundamental relation. Arp72d has a low oxygen abundance, even for its mass, although the uncertainty in the oxygen abundance value is very high and it could still be a detached TDG. Arp72c oxygen abundance is not possible to determine due to the lack of [NII]6583 line detection, but since the stellar metallicity is large, we conclude that is in fact a detached TDG.

In conclusion, there is evidence from the Mass-Metallicity and Mass-Oxygen abundance relations that the five least massive objects are detached TDGs since either the stellar metallicity or the nebular oxygen abundance is high in comparison with other dwarf galaxies. The most massive object, Arp86a, has the

**Table 2.** Extinction corrected emission line fluxes for the confirmed detached TDGs and the Arp72 system smaller companion, NGC 5994. Fluxes are in units of $10^{-17}$ erg/s/cm$^2$. Color excess and oxygen abundance are also included.

| Name | H$\alpha$ | H$\beta$ | [OIII]4959 | [OIII]5007 | [NII]6548 | [NII]6583 | [SII]6717 | [SII]6731 | $E(B-V)$ | 12+log(O/H) |
|---|---|---|---|---|---|---|---|---|---|---|
| Arp65a | 14.6 ± 1.2 | 5.4 ± 1.4 | ... | 6.4 ± 1.3 | ... | 5.9 ± 1.2 | 4.8 ± 1.2 | 4.3 ± 1.4 | ... | 8.5 ± 0.7 |
| Arp72a | 176.4 ± 0.8 | 63.2 ± 1.1 | 47.7 ± 1.1 | 132.2 ± 1.0 | 4.6 ± 0.8 | 13.8 ± 0.8 | 20.6 ± 0.9 | 19.8 ± 0.9 | ... | 8.14 ± 0.1 |
| Arp72b | 1693.5 ± 2.0 | 591.4 ± 2.3 | 977.3 ± 2.2 | 3132.7 ± 2.2 | ... | 63.4 ± 2.3 | 59.7 ± 2.1 | 36.5 ± 1.6 | 0.524 ± 0.009 | 8.14 ± 0.16 |
| Arp72c | 35.1 ± 1.6 | 19.0 ± 2.2 | 13.7 ± 2.2 | 19.9 ± 2.0 | ... | ... | ... | ... | ... | ... |
| Arp72d | 42.3 ± 1.6 | 18.4 ± 1.8 | 5.62 ± 0.09 | 17.02 ± 0.09 | ... | 2.3 ± 0.4 | 6.15 ± 0.16 | 4.47 ± 0.22 | ... | 7.5 ± 1.0 |
| NGC5994 | 2831 ± 4 | 989 ± 5 | 769 ± 5 | 2241 ± 5 | 55.6 ± 3.2 | 316 ± 4 | 605 ± 4 | 463 ± 5 | 0.372 ± 0.007 | 8.21 ± 0.05 |
| Arp86a | 620 ± 4 | 217 ± 4 | 46.5 ± 3.4 | 173 ± 4 | 82 ± 5 | 184 ± 4 | 158 ± 4 | 110 ± 4 | 0.233 ± 0.020 | 8.43 ± 0.07 |
| Arp86d | 73.5 ± 1.9 | 25.7 ± 1.7 | 18.1 ± 1.7 | 45.9 ± 1.6 | 7.5 ± 2.2 | 14.3 ± 1.9 | 21.7 ± 1.8 | 4.1 ± 1.2 | 0.11 ± 0.05 | 8.3 ± 0.4 |

**Table 3.** GALEX, *Spitzer*, and DESI-LIS photometry of the spectroscopically confirmed detached TDGs.

| id | FUV mJy | NUV mJy | $u$ (SDSS) mJy | $g$ (SDSS) mJy | $r$ (SDSS) mJy | $i$ (SDSS) mJy | $z$ (SDSS) mJy | |
|---|---|---|---|---|---|---|---|---|
| Arp65a | 0.00989 ± 0.00026 | 0.00863 ± 0.00032 | <0.03 | 0.0119 ± 0.0021 | <0.01 | <0.03 | <0.08 | |
| Arp72a | 0.0353 ± 0.0005 | 0.0323 ± 0.0004 | 0.042 ± 0.008 | 0.0623 ± 0.0027 | 0.082 ± 0.004 | 0.069 ± 0.007 | <0.1 | |
| Arp72b | 0.01165 ± 0.00032 | 0.01105 ± 0.00031 | <0.06 | 0.0713 ± 0.0025 | 0.063 ± 0.004 | 0.067 ± 0.007 | <0.1 | |
| Arp72c | 0.01067 ± 0.00031 | 0.00934 ± 0.00033 | <0.03 | 0.0139 ± 0.0019 | 0.0106 ± 0.0031 | <0.03 | <0.07 | |
| Arp72d | 0.04851 ± 0.00033 | 0.05901 ± 0.00035 | 0.167 ± 0.008 | 0.2948 ± 0.0024 | 0.354 ± 0.004 | 0.387 ± 0.006 | 0.391 ± 0.033 | |
| Arp86a | 0.03722 ± 0.00032 | 0.0428 ± 0.0005 | 0.190 ± 0.004 | 0.6289 ± 0.0016 | 1.1099 ± 0.0030 | 1.422 ± 0.005 | 1.756 ± 0.019 | |
| Arp86d | 0.0128 ± 0.0004 | 0.0125 ± 0.0005 | <0.03 | 0.0128 ± 0.0017 | <0.04 | <0.06 | <0.2 | |
| id | $g$ (DES) mJy | $r$ (DES) mJy | $z$ (DES) mJy | 3.6 μm mJy | 4.5 μm mJy | 5.8 μm mJy | 8.0 μm mJy | 24 μm mJy |
| Arp65a | 0.0086 ± 0.0005 | 0.0095 ± 0.0008 | 0.0094 ± 0.0022 | 0.0321 ± 0.0018 | 0.0197 ± 0.0022 | 0.046 ± 0.010 | 0.113 ± 0.008 | <0.2 |
| Arp72a | 0.0754 ± 0.0008 | 0.0931 ± 0.0015 | 0.108 ± 0.004 | 0.0408 ± 0.0019 | 0.0208 ± 0.0022 | <0.02 | 0.039 ± 0.009 | <0.1 |
| Arp72b | 0.0508 ± 0.0007 | 0.0693 ± 0.0014 | 0.081 ± 0.004 | 0.0255 ± 0.0016 | 0.0174 ± 0.0020 | 0.065 ± 0.008 | 0.053 ± 0.008 | 0.23 ± 0.04 |
| Arp72c | 0.0194 ± 0.0011 | 0.0222 ± 0.0021 | <0.02 | 0.0166 ± 0.0015 | <0.006 | <0.02 | 0.038 ± 0.008 | <0.1 |
| Arp72d | 0.2827 ± 0.0007 | 0.3652 ± 0.0014 | 0.408 ± 0.004 | ... | ... | ... | ... | ... |
| Arp86a | 0.6608 ± 0.0005 | 1.1842 ± 0.0014 | 1.7109 ± 0.0025 | 0.9117 ± 0.0019 | 0.5463 ± 0.0024 | 0.684 ± 0.011 | 1.200 ± 0.011 | 0.96 ± 0.07 |
| Arp86d | 0.0160 ± 0.0005 | 0.0182 ± 0.0012 | <0.008 | 0.0241 ± 0.0020 | 0.0123 ± 0.0025 | 0.081 ± 0.012 | 0.110 ± 0.014 | <0.2 |

**Table 4.** CIGALE input parameters..

| | |
|---|---|
| Free parameters | |
| $e$-folding time of the old population | 1, 2, 3, 4, 5 Gyr |
| $e$-folding time of the late starburst population | 25, 50, 100, 125, 150, 175, 200, 250, 300, 400, 500 Myr |
| Mass fraction of the late burst population | 0.1, 0.2, 0.3, 0.4, 0.5, 0.6, 0.7, 0.8, 0.9 |
| Age of the late burst | 25, 50, 100, 150, 200, 300, 400, 500, 600, 700, 800, 900, 1000, 1250, 1500, 2000 Myr |
| Metallicity | 0.0001, 0.0004, 0.004, 0.008, 0.02, 0.05 |
| $E(B-V)$ of the stellar continuum light for the young population. | 0.01, 0.02, 0.03, 0.04, 0.05, 0.06 mag |
| Mass fraction of PAH | 0.47, 1.12, 3.19, 5.26, 7.32 |
| Powerlaw slope $\mathrm{d}U/\mathrm{d}M \propto U^{\alpha}$ | 1, 2, 3 |
| Fraction illuminated from minimum to maximum radiation field | 0.0, 0.25, 0.5, 0.75, 1.0 |
| Minimum radiation field | 0.1, 0.4, 0.8, 1, 2, 4, 8, 12, 17, 20, 25, 30, 50 |
| Fixed parameters | |
| Age of the oldest stars | 11 Gyr |
| Reduction factor for the $E(B-V)$ of the old population compared to the young one | 0.5 |
| Central wavelength of the UV bump | 217.5 nm |
| Amplitude of the UV bump | 35 nm |
| Slope $\delta$ of the power law modifying the attenuation curve | 0 |
| IMF | Chabrier (2003) |

expected metallicity and oxygen nebular abundance for a dwarf galaxy, while Arp72d has very large uncertainties in these values, so we cannot conclude one way or the other.

### 7.2. Oxygen abundance gradients

Another test of the TDG hypothesis is comparison with metallicities within the disks of the galaxies. We used the homogenized HyperLeda database[5] to obtain the inclination of the main galaxies. We took these inclinations into account when estimating the galactocentric radius for each spaxel in the MUSE data for Arp 72 and in each region reported in Zhou et al. (2014) and Zasov et al. (2020). For Arp 65, we assumed that NGC 90, the spiral to the west, is the parent galaxy. The oxygen abundance gradients for each interacting system are plotted in Fig. 8, where the detached TDGs are shown as star symbols. All the TDGs exhibit an oxygen abundance consistent with the gradient of the main galaxy, that is, the measured abundance is approximately the expected one for the radii where the TDGs are located, except

[5] http://leda.univ-lyon1.fr/

**Table 5.** Results from CIGALE fits.

| id | $M_*$ $M_\odot$ | $Z$ | SFR $M_\odot$/yr | $f_{burst}$ [(a)] | Burst age Myr |
|---|---|---|---|---|---|
| Arp65a | $(1.7 \pm 1.1) \times 10^6$ | $0.023 \pm 0.019$ | $0.0060 \pm 0.0009$ | $0.47 \pm 0.26$ | $(1.1 \pm 0.5) \times 10^2$ |
| Arp72a | $(1.2 \pm 0.4) \times 10^7$ | $0.007 \pm 0.005$ | $0.0060 \pm 0.0013$ | $0.41 \pm 0.25$ | $(4.3 \pm 1.5) \times 10^2$ |
| Arp72b | $(1.7 \pm 0.5) \times 10^7$ | $0.0005 \pm 0.0009$ | $0.0010 \pm 0.0004$ | $0.36 \pm 0.23$ | $(8.7 \pm 3.3) \times 10^2$ |
| Arp72c | $(2.5 \pm 1.3) \times 10^6$ | $0.034 \pm 0.018$ | $0.0021 \pm 0.0004$ | $0.45 \pm 0.26$ | $(3.2 \pm 1.1) \times 10^2$ |
| Arp72d | $(8.4 \pm 2.7) \times 10^7$ | $0.001 \pm 0.004$ | $0.0034 \pm 0.0020$ | $0.46 \pm 0.24$ | $(8.7 \pm 3.3) \times 10^2$ |
| Arp86a | $(1.09 \pm 0.20) \times 10^9$ | $0.0060 \pm 0.0025$ | $0.0173 \pm 0.0032$ | $0.29 \pm 0.17$ | $(1.85 \pm 0.27) \times 10^3$ |
| Arp86d | $(3.6 \pm 2.2) \times 10^6$ | $0.023 \pm 0.019$ | $0.0068 \pm 0.0015$ | $0.42 \pm 0.27$ | $(1.7 \pm 0.6) \times 10^2$ |

**Notes.** [(a)]Fraction of stars formed in the recent burst relative to the total mass of stars ever formed.

in the case of Arp86, where the oxygen abundances exhibit too much dispersion to visualize any gradient. However, the oxygen abundance values in Arp86 are within the observed range in the main galaxy and tails. In the case of Arp72d, which is at a deprojected distance of 150 kpc, the oxygen abundance is lower than expected from the observed gradient in Arp72, although the uncertainty is large due to the faint detection of the [NII] emission line, so the oxygen abundance could be compatible with that of the disk.

### 7.3. The effective radii of the tidal dwarf galaxies

Duc et al. (2014) suggest that TDGs have larger effective radii relative to their stellar masses, compared to other dwarf galaxies. This means that effective radii may be a powerful tool for identifying detached TDGs. The nearness of our sample galaxies and the availability of DESI-LIS images makes such an analysis possible. At the distance of our objects, the median DESI-LIS seeing of 1.″1 FWHM (Dey et al. 2019) corresponds to 0.3 kpc, and thus regions that have diameters of 1–2 kpc are well resolved.

We used the DESI-LIS $r$ images to determine the effective radii (half-light radii) of the candidate TDGs. These radii are provided in Table 6. In Figure 9, we plot these effective radii (red filled triangles) against the stellar masses, and compare with effective radii of other candidate TDGs from earlier studies (Duc et al. 2014; Lee-Waddell et al. 2016; Román et al. 2021; Gray et al. 2023). In Figure 9, we also plot Local Group dwarf Irregular galaxies (dIrr, green open circles) and dwarf spheroidal (dSph) or dSph/dIrr galaxies from McConnachie (2012) and the Eigenthaler et al. (2018) Fornax dwarf galaxies. We also show the best effective radii-stellar mass fits from Lange et al. (2016) as green dashed line (Sd-Irr galaxies), brown dashed line (Sab-Scd galaxies), and olive dot-dash line (S0-Sa galaxies).

Figure 9 shows that Arp 86a is relatively compact for its stellar mass respect to other TDGs, and is similar in size with S0-Sa galaxies from Lange et al. (2016) (olive line), consistent with our conclusion based on metallicity that it is probably a preexisting dwarf galaxy rather than a TDG. In contrast, our other candidate TDGs are larger than most Local Group dIrr galaxies with the same stellar mass, are more similar in size to Local Group dSph galaxies with similar masses, and lie above the extrapolation of the Sd-Irr relation from Lange et al. (2016) to low masses (green line). For a given stellar mass, the TDGs in our sample lie at the upper edge of the size range of Fornax dwarf galaxies. The five confirmed TDGs can be split into two groups of stellar mass: one that is less massive within the $\log(M_*) = [6.2, 6.6]$ range (Arp65a, Arp72c, and Arp86d) and another that is more massive within the $\log(M_*) = [7.1, 7.2]$ range (Arp72a and Arp72b). In the less-massive range, the average effective radius of dwarf galaxies from Eigenthaler et al. (2018) is $370 \pm 50$ pc, while the effective radius of the less-massive detached TDGs from this work are larger (see Table 6). In the more-massive range, the average effective radius of dwarf galaxies from Eigenthaler et al. (2018) is $680 \pm 110$ pc, while the sizes of the more-massive detached TDGs from this work are also larger (see Table 6).

The confirmed TDGs in this work, with stellar masses $M_* < 1.7 \times 10^7\,M_\odot$, are less massive than most previously known TDGs; only three of the twelve previously identified TDGs in Figure 9 have masses $M_* < 10^7\,M_\odot$. Our confirmed TDGs have effective radii $R_{\rm eff} < 1.10$ kpc, so they are smaller than the previous identified TDGs, except one detected from the Arecibo Legacy Fast ALFA (ALFALFA) survey.

## 8. Discussion

The spectral resolution of the observations, 4.4 Å, corresponds to a velocity resolution of about 200 km s$^{-1}$ at H$\alpha$. This is too large to allow for reliable measurement of the rotation curves of these TDGs; thus, we could not directly measure the dynamical masses. That means we cannot test directly for the presence (or absence) of Dark Matter in the TDGs. However, we can address this issue indirectly, via the timescale of star formation triggering. According to simulations by Lelli et al. (2015), dynamical equilibrium is achieved in gas-dominated TDGs within 200 Myr. This means that all six of our detached TDGs should be either in or very close to dynamical equilibrium, assuming that the TDGs formed simultaneously with the star formation burst. If the TDGs are in dynamical equilibrium, the dynamical mass should be equal to the total mass (baryonic plus Dark Matter).

The survival timescale of TDGs is crucial for understanding their implications in galaxy evolution and interpreting observations in terms of dark galaxies (Román et al. 2021). Our burst ages indicate that TDGs can survive for at least 900 Myr, as observed in the case of Arp72b. We note that this represents a lower limit to the possible ages of TDGs since our observations are biased toward emission line-emitting objects because we used the H$\alpha$ line for redshift confirmation. It is possible that TDGs can survive even longer than what we have observed in this sample.

Haslbauer et al. (2019) reported that gas-rich TDGs from the Illustris-1 simulation do not have Dark Matter, are gravitationally bound, and are in virial equilibrium. Our TDGs, selected because they show star formation and nebular emission lines, are gas-rich. Consequently, they should be compared with the gas-rich TDGs from (2019, sample B). Their stellar masses and ages are close to those in Sample B, which have median values of

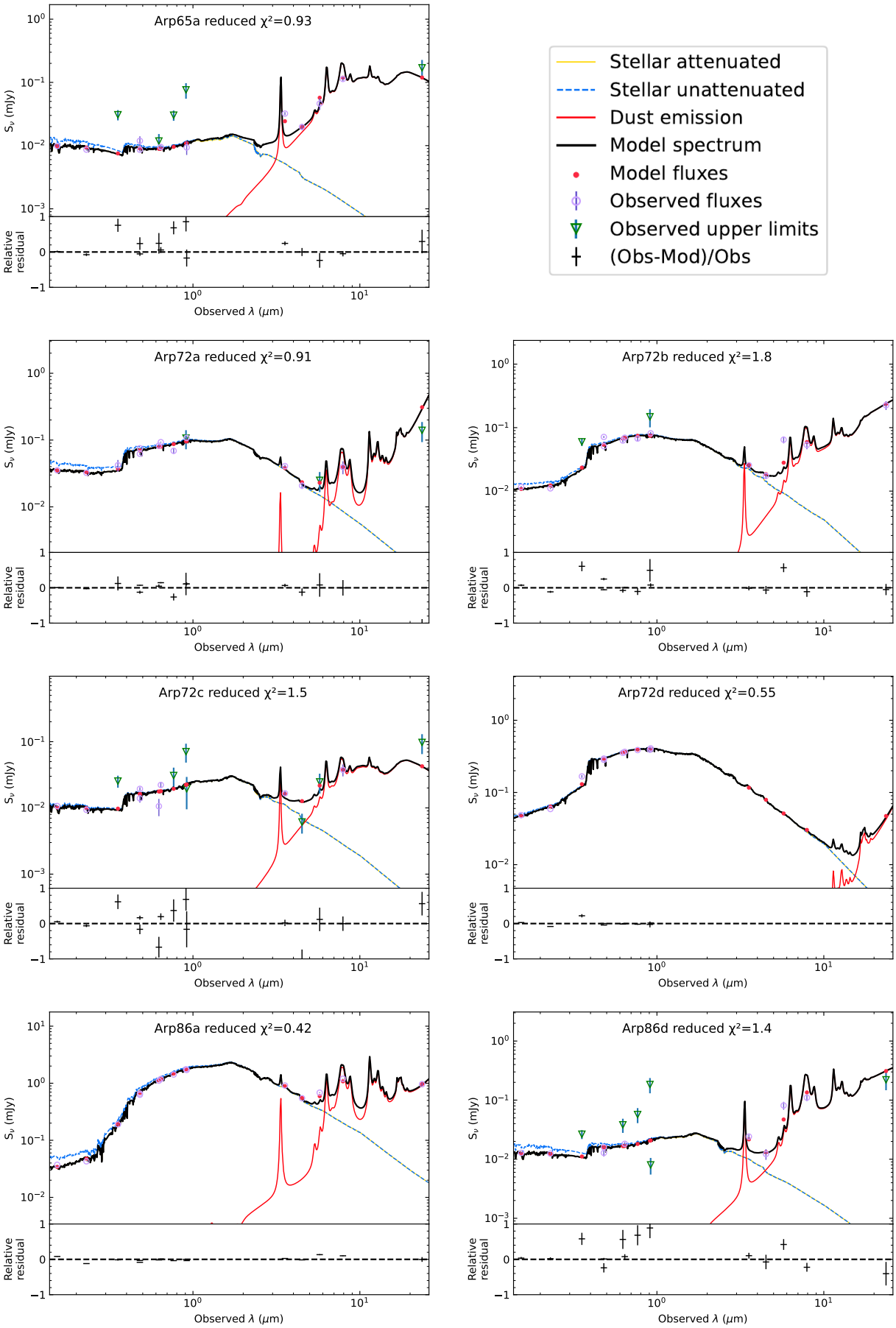


**Fig. 5.** Spectral energy distributions of the seven spectroscopically confirmed TDGs. We show the fitted model using CIGALE as black lines.

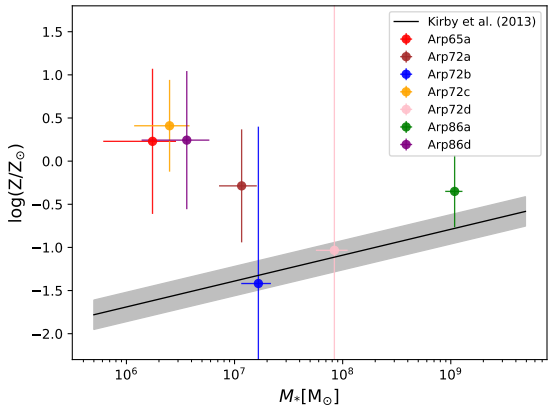


**Fig. 6.** Stellar metallicity versus stellar mass for the six redshift confirmed TDGs. The fundamental relation for dwarf galaxies obtained from Kirby et al. (2013) is shown as a black line. The gray shaded range marks the rms spread in the best-fit relation. The metallicity of the Sun is set to $Z_\odot = 0.134$ (Asplund et al. 2009).

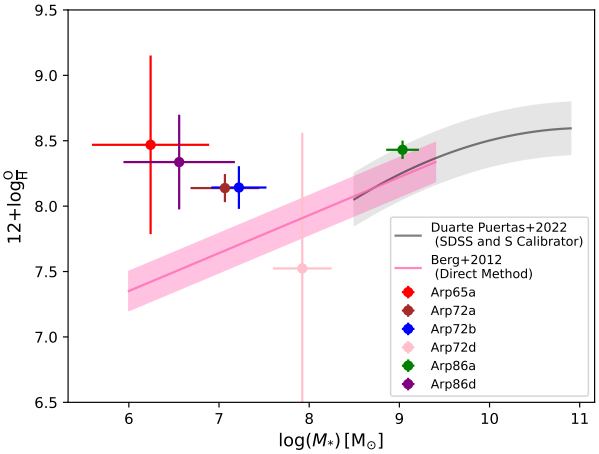


**Fig. 7.** Nebular oxygen abundance versus stellar mass for the six spectroscopically confirmed TDGs. No oxygen abundance is available for Arp72c. The fundamental relation for star-forming SDSS galaxies with log $M* > 8.5$ from Duarte Puertas et al. (2022) is shown as a black solid line. The gray shaded range marks the rms spread in the best-fit relation. Dwarf galaxy relation from Berg et al. (2012) is shown in pink.

$3\times10^6$ $M_\odot$ and 1 Gyr. In the Illustris-1 simulation, a "stellar mass particle" has a mass of $1.26 \times 10^6$ $M_\odot$, and thus such low-mass TDGs are not well resolved in the simulation. Ploeckinger et al. (2018) reported gas-rich TDG candidates and Dark Matter-free objects detected in the Evolution and Assembly of GaLaxies and their Environments (EAGLE) cosmological simulation, having a mean stellar mass of $2 \times 10^6$ $M_\odot$, also in agreement with the values we find in this study. A "stellar mass particle" in the EAGLE simulation is $2.26 \times 10^5$ $M_\odot$. Although TDGs do not have Dark Matter, the use of gas dynamics to test different cosmological scenarios can be problematic if the gas is not in virial equilibrium (Flores et al. 2016). The best TDGs to examine for the presence and effects of Dark Matter are those from Arp72, as they are old enough to be in equilibrium.

### *Comparison to other studies*

To investigate the longevity of TDGs, Bournaud & Duc (2006) ran 96 $N$-body simulations of galaxy interactions with a range

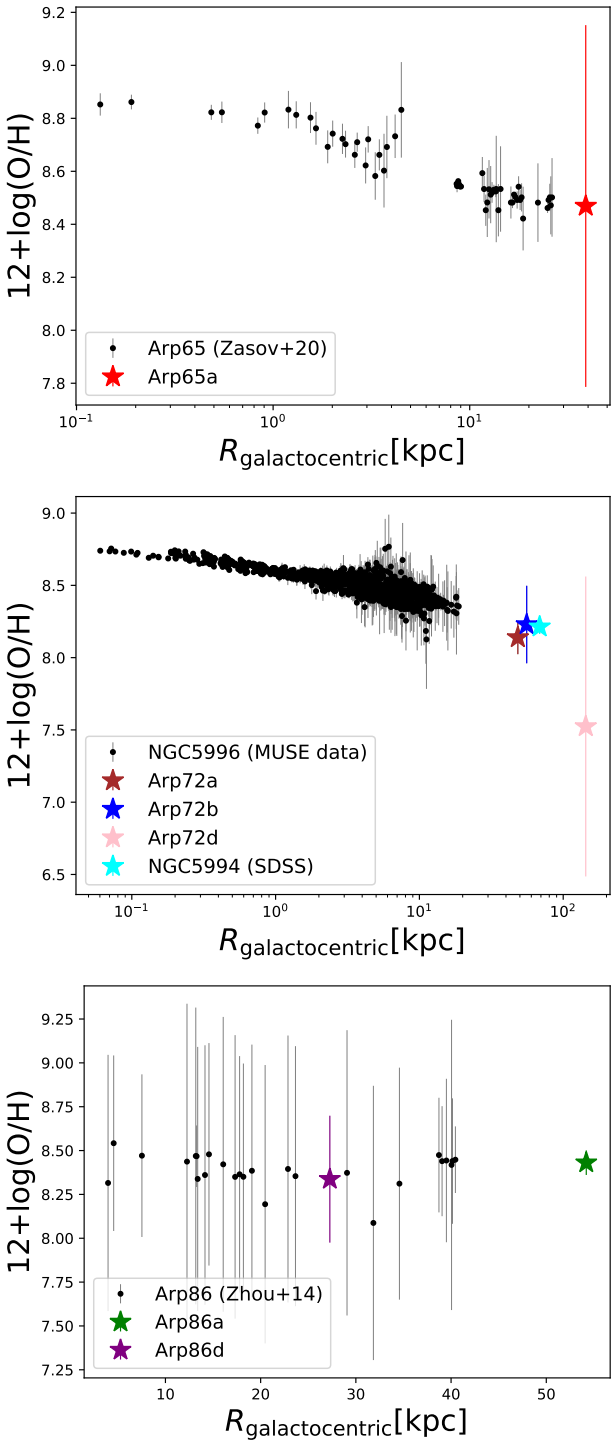


**Fig. 8.** Oxygen abundance versus galactocentric radius for the six spectroscopically confirmed TDGs (colored star symbols). We show the nebular regions along the host galaxies as black dots and as a cyan star for NGC5994 (middle pannel).

of mass ratios and orbital parameters. About 75% of the TDGs formed in these simulations either fell back onto their parent galaxies or became disrupted within 300 Myr. According to their models, long-lasting TDGs are more likely to form in prograde encounters between approximately equal mass galaxies. Bournaud & Duc (2006) concluded that pairs with mass ratios between 1/4 and 8 are the most favorable for the production of long-lived TDGs.

**Table 6.** Effective radii in the *r* band of the detached TDG candidates.

| Name | $R_{\rm eff\,r}$ kpc |
|---|---|
| Arp65a | 0.89 |
| Arp72a | 0.87 |
| Arp72b | 1.10 |
| Arp72c | 0.69 |
| Arp72d | 1.42 |
| Arp86a | 1.48 |
| Arp86d | 0.49 |

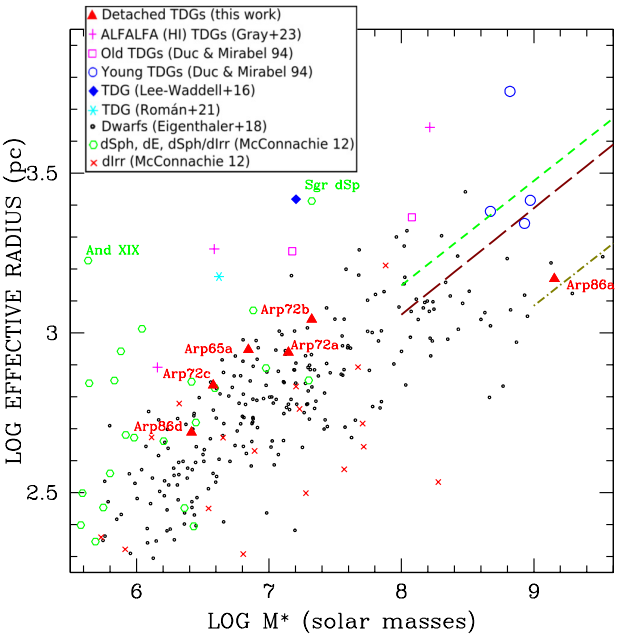


**Fig. 9.** Effective radii versus stellar mass. Red filled triangles are our candidate TDGs. Magenta crosses are ALFALFA-selected candidate TDGs from Gray et al. (2023). Magenta open squares are candidate old TDGs from Duc & Mirabel (1994); Blue open circles are young TDGs in tidal features, as tabulated by Duc & Mirabel (1994). Blue filled diamond is the TDG AGC 208457, from Lee-Waddell et al. (2016). Cyan asterisk is the candidate TDG from Román et al. (2021). Small black dots are dwarf galaxies in the Fornax cluster, from Eigenthaler et al. (2018). Small green open hexagons are Local Group dSph, dE, dSph/dIrr, from McConnachie (2012). Red x marks are Local Group dwarf Irregular galaxies, from McConnachie (2012). The two largest Local Group galaxies are labeled in green. Best effective radii-stellar mass fits from Lange et al. (2016) are shown as green dashed line (Sd-Irr galaxies), brown dashed line (Sab-Scd galaxies), and olive dot-dash line (S0-Sa galaxies).

Two out of the three systems in which we find detached TDGs, Arp 72 and Arp 86, have companions with lower masses than expected based on these models. If 3.6 µm flux ratio is that of the stellar massz, the mass ratio of Arp72 (1/12) is rather different from what is reported by Bournaud & Duc (2006), which suggests that the detached TDGs from Arp 72 are probably different from those studied in the simulations of Bournaud & Duc (2006).

Previous studies have tried to discover detached TDGs. Using optical and HI imaging, Duc et al. (2014) obtained optical spectra of seven dwarf galaxy-like objects close to nearby early-type galaxies. If these early-type galaxies are the relics of galaxy mergers, some of these dwarfs may have been formed tidally. One of their candidate TDGs appears to be connected to a nearby elliptical galaxy by a faint tidal tail, and it has a higher metallicity than expected given its stellar mass, suggesting a tidal origin.

Delgado-Donate et al. (2003) obtained deep optical images of six merger remnants, searching for possible detached TDGs in their vicinities. Their statistics were consistent with expected number counts of background galaxies, and they concluded that there is no evidence for a large population of locally formed dwarf galaxies near those galaxies. More recently, Gray et al. (2023) confirmed two detached TDGs based on HI observations from the ALFALFA survey and deep optical imaging.

Detached TDGs do not seem to be very common, although they could be more frequent but difficult to detect due to their brightness and the limited spatial field of view of spectroscopic and optical observations. Wide surveys will help improve the spatial coverage of nearby galaxy mergers, where detached TDG candidates can be detected. However, spectroscopic observations would still be needed to confirm the membership of the TDG candidates to galaxy mergers. Wide surveys such as Javalambre Physics of the Accelerating Universe (J-PAS, Benitez et al. 2014; Bonoli et al. 2021) will cover 8500 deg$^2$ in 54 narrowband filters with a pseudo spectral resolution of $R \sim 40$, where redshift confirmation will be possible for detached TDG characterization studies thereafter. Therefore, we will be able to improve the detections of these detached TDGs in order to have a complete census from which to estimate formation and survival rates. In turn, this will allow us to understand the impact of TDGs on galaxy evolution and dwarf galaxy formation. It will also allow us to identify the best candidates for detailed follow-up studies. The Baryonic Tully-Fisher Relation (BTFR), which relates the baryonic mass with the rotation velocity of galaxies, has been postulated as a fundamental relation (McGaugh et al. 2000; McGaugh 2005; Lelli et al. 2019). However, due to the complexity of dynamical modeling of faint dwarf galaxies with turbulent gas, the origin of a possible deviation from the BTFR relation of TDGs (or other dwarf galaxies) is still an open question (Lelli et al. 2015; Guo et al. 2020; Du et al. 2024).

Detailed dynamical analysis of detached TDGs could be used to test the validity of the BTFR for TDGs. Since they are already detached from the main galaxies, they should be simpler to analyze from a dynamical perspective and thus can be used to test the different predictions for the BTFR from various theories (Lelli et al. 2019). The presence of any dynamically measured amount of nonvisible matter in TDGs has implications for the distribution of dark matter or the existence of dark gas (Lelli et al. 2015).

Stellar feedback is commonly invoked as one of the drivers of stellar mass-growth regulation in the Λ Cold Dark Matter (Λ-CDM) standard cosmological model (Silk & Mamon 2012). Dark matter deficient galaxies such as TDGs should experience stronger stellar feedback due to the lack of mass compared to dark matter dominated dwarf galaxies. Detailed analyses of detached TDGs, such as those using chemical enrichment histories (Lilly et al. 2013; Barrera-Ballesteros et al. 2018) or star formation histories (Zaragoza-Cardiel et al. 2019, 2020), can impose constraints on the stellar feedback needed to match the predicted relations from Λ-CDM galaxy simulations.

## 9. Conclusions

In our search for detached TDGs associated with a sample of 39 interacting galaxies, we spectroscopically confirmed the

redshifts of seven detached TDG candidates. For six of these objects, we utilized the Boller and Chivens long-slit spectrograph at the 2.1m telescope at the San Pedro Mártir Observatory. We used an SDSS spectrum for the seventh source. Nebular oxygen abundances were derived using the S-calibrator from Pilyugin & Grebel (2016), and stellar metallicities, masses, and recent burst ages were determined through SED fitting using CIGALE (Boquien et al. 2019). Based on the fundamental stellar and gas metallicity-stellar mass relations, we confirmed the tidal nature of five out of the seven detached TDG candidates. One candidate, Arp72d, remains uncertain due to high uncertainties in nebular abundance and stellar metallicity, while the most massive one, Arp86a, is compatible with being a preexisting dwarf galaxy.

We compared the nebular oxygen abundances of the seven TDG candidates with the (O/H)-to-galactocentric radius relation of the host galaxies. The TDG candidates exhibit oxygen abundances consistent with the observed abundance gradients in the host galaxies. The effective radii-stellar mass relation of these detached TDGs indicates that they tend to be larger than typical dwarf galaxies on average, while they are smaller than other TDGs for a given mass. The most massive TDG candidate, Arp86a, is more compact relative to its mass and is consistent in size with other dwarf galaxies of its mass, supporting the idea that it is a preexisting dwarf galaxy rather than a TDG.

Two of the interacting galaxy systems, Arp72 and Arp86, have merger ratios of approximately 1/10 and 1/5, respectively. This contrasts with $N$-body simulations (Bournaud & Duc 2006), which suggest that detached TDGs have a higher survival probability for merger ratios between 1/4 and 8/1, indicating potential differences in formation and survival mechanisms.

The detection and study of detached TDGs has significant implications for dwarf galaxy formation and the discovery of so-called dark galaxies, that is, dark matter halos that were unable to transform their gas into stars. The optical brightnesses of TDGs decreases with time, so if detached TDGs are frequent, have large survival times, and become gravitationally unbound from the main galaxies, it is probable that many identified as dark galaxies are indeed detached TDGs. However, limitations in depth and field of view of observations raise questions about the low number of detections, whether due to actual scarcity or observational factors. The confirmed detached TDGs presented in this work offer valuable opportunities for studying TDG evolution, star formation in extreme environments, dwarf galaxy formation, and the testing of Λ-CDM predictions regarding the BTFR, stellar feedback, and the distribution of dark matter.

## Data availability

Reduced spectroscopic data are available at the CDS via anonymous ftp to cdsarc.cds.unistra.fr (130.79.128.5) or via https://cdsarc.cds.unistra.fr/viz-bin/cat/J/A+A/689/A206

*Acknowledgements.* Based upon observations carried out at the Observatorio Astronómico Nacional on the Sierra San Pedro Mártir (OAN-SPM), Baja California, México. We thank the daytime and night support staff at the OAN-SPM for facilitating and helping obtain our observations. JZC acknowledges the financial support provided by the Instituto Nacional de Astrofísica, Óptica y Electrónica, and the Governments of Spain and Aragón through their general budgets and the Fondo de Inversiones de Teruel. BJS and MLG were supported by National Science Foundation Extragalactic Astronomy grant ASTR-1714491 and from the NASA Tennessee Space Grant. We would like to express our gratitude to the anonymous referee for their valuable comments and suggestions, which have significantly improved the quality of this paper. Their thorough review and constructive feedback were greatly appreciated. This research has made use of the NASA/IPAC Extragalatic Database (NED), which is operated by the Jet Propulsion Laboratory, California Institute of Technology, under contract with NASA. This work is based in part on observations made with the *Spitzer* Space Telescope, which is operated by the Jet Propulsion Laboratory (JPL), California Institute of Technology under a contract with NASA. This study also uses data from the NASA Galaxy Evolution Explorer (GALEX), which was operated for NASA by the California Institute of Technology under NASA contract NAS5-98034. We acknowledge the usage of the HyperLeda database (http://leda.univ-lyon1.fr) Based on observations collected at the European Southern Observatory under ESO programme 0101.D-0748(B) and data obtained from the ESO Science Archive Facility with DOI under https://doi.org/10.18727/archive/41. The Legacy Surveys consist of three individual and complementary projects: the Dark Energy Camera Legacy Survey (DECaLS; Proposal ID #2014B-0404; PIs: David Schlegel and Arjun Dey), the Beijing-Arizona Sky Survey (BASS; NOAO Prop. ID #2015A-0801; PIs: Zhou Xu and Xiaohui Fan), and the Mayall $z$-band Legacy Survey (MzLS; Prop. ID #2016A-0453; PI: Arjun Dey). DECaLS, BASS and MzLS together include data obtained, respectively, at the Blanco telescope, Cerro Tololo Inter-American Observatory, NSF's NOIRLab; the Bok telescope, Steward Observatory, University of Arizona; and the Mayall telescope, Kitt Peak National Observatory, NOIRLab. Pipeline processing and analyses of the data were supported by NOIRLab and the Lawrence Berkeley National Laboratory (LBNL). The Legacy Surveys project is honored to be permitted to conduct astronomical research on Iolkam Du'ag (Kitt Peak), a mountain with particular significance to the Tohono O'odham Nation. NOIRLab is operated by the Association of Universities for Research in Astronomy (AURA) under a cooperative agreement with the National Science Foundation. LBNL is managed by the Regents of the University of California under contract to the U.S. Department of Energy. This project used data obtained with the Dark Energy Camera (DECam), which was constructed by the Dark Energy Survey (DES) collaboration. Funding for the DES Projects has been provided by the U.S. Department of Energy, the U.S. National Science Foundation, the Ministry of Science and Education of Spain, the Science and Technology Facilities Council of the United Kingdom, the Higher Education Funding Council for England, the National Center for Supercomputing Applications at the University of Illinois at Urbana-Champaign, the Kavli Institute of Cosmological Physics at the University of Chicago, Center for Cosmology and Astro-Particle Physics at the Ohio State University, the Mitchell Institute for Fundamental Physics and Astronomy at Texas A&M University, Financiadora de Estudos e Projetos, Fundacao Carlos Chagas Filho de Amparo, Financiadora de Estudos e Projetos, Fundacao Carlos Chagas Filho de Amparo a Pesquisa do Estado do Rio de Janeiro, Conselho Nacional de Desenvolvimento Cientifico e Tecnologico and the Ministerio da Ciencia, Tecnologia e Inovacao, the Deutsche Forschungsgemeinschaft and the Collaborating Institutions in the Dark Energy Survey. The Collaborating Institutions are Argonne National Laboratory, the University of California at Santa Cruz, the University of Cambridge, Centro de Investigaciones Energeticas, Medioambientales y Tecnologicas-Madrid, the University of Chicago, University College London, the DES-Brazil Consortium, the University of Edinburgh, the Eidgenossische Technische Hochschule (ETH) Zurich, Fermi National Accelerator Laboratory, the University of Illinois at Urbana-Champaign, the Institut de Ciencies de l'Espai (IEEC/CSIC), the Institut de Fisica d'Altes Energies, Lawrence Berkeley National Laboratory, the Ludwig Maximilians Universitat Munchen and the associated Excellence Cluster Universe, the University of Michigan, NSF's NOIRLab, the University of Nottingham, the Ohio State University, the University of Pennsylvania, the University of Portsmouth, SLAC National Accelerator Laboratory, Stanford University, the University of Sussex, and Texas A&M University. BASS is a key project of the Telescope Access Program (TAP), which has been funded by the National Astronomical Observatories of China, the Chinese Academy of Sciences (the Strategic Priority Research Program "The Emergence of Cosmological Structures" Grant # XDB09000000), and the Special Fund for Astronomy from the Ministry of Finance. The BASS is also supported by the External Cooperation Program of Chinese Academy of Sciences (Grant # 114A11KYSB20160057), and Chinese National Natural Science Foundation (Grant # 12120101003, # 11433005). The Legacy Survey team makes use of data products from the Near-Earth Object Wide-field Infrared Survey Explorer (NEOWISE), which is a project of the Jet Propulsion Laboratory/California Institute of Technology. NEOWISE is funded by the National Aeronautics and Space Administration. The Legacy Surveys imaging of the DESI footprint is supported by the Director, Office of Science, Office of High Energy Physics of the U.S. Department of Energy under Contract No. DE-AC02-05CH1123, by the National Energy Research Scientific Computing Center, a DOE Office of Science User Facility under the same contract; and by the U.S. National Science Foundation, Division of Astronomical Sciences under Contract No. AST-0950945 to NOAO. Funding for the Sloan Digital Sky Survey IV has been provided by the Alfred P. Sloan Foundation, the U.S. Department of Energy Office of Science, and the Participating Institutions. SDSS acknowledges support and resources from the Center for High-Performance Computing at the University of Utah.

The SDSS web site is www.sdss4.org. SDSS is managed by the Astrophysical Research Consortium for the Participating Institutions of the SDSS Collaboration including the Brazilian Participation Group, the Carnegie Institution for Science, Carnegie Mellon University, Center for Astrophysics – Harvard & Smithsonian (CfA), the Chilean Participation Group, the French Participation Group, Instituto de Astrofísica de Canarias, The Johns Hopkins University, Kavli Institute for the Physics and Mathematics of the Universe (IPMU)/University of Tokyo, the Korean Participation Group, Lawrence Berkeley National Laboratory, Leibniz Institut für Astrophysik Potsdam (AIP), Max-Planck-Institut für Astronomie (MPIA Heidelberg), Max-Planck-Institut für Astrophysik (MPA Garching), Max-Planck-Institut für Extraterrestrische Physik (MPE), National Astronomical Observatories of China, New Mexico State University, New York University, University of Notre Dame, Observatório Nacional/MCTI, The Ohio State University, Pennsylvania State University, Shanghai Astronomical Observatory, United Kingdom Participation Group, Universidad Nacional Autónoma de México, University of Arizona, University of Colorado Boulder, University of Oxford, University of Portsmouth, University of Utah, University of Virginia, University of Washington, University of Wisconsin, Vanderbilt University, and Yale University.

## References

Ahumada, R., Allende, Prieto C., Almeida, A., et al. 2020, ApJS, 249, 3
Asplund, M., Grevesse, N., Sauval, A. J., et al. 2009, ARA&A, 47, 481
Astropy Collaboration (Price-Whelan, A. M., et al.) 2022, ApJ, 935, 167
Bacon, R., Accardo, M., Adjali, L., et al. 2010, SPIE Conf. Ser., 7735, 773508
Barnes, J. E., & Hernquist, L. 1992, Nature, 360, 715
Barrera-Ballesteros, J. K., Heckman, T., Sánchez, S. F., et al. 2018, ApJ, 852, 74
Benitez, N., Dupke, R., Moles, M., et al. 2014, ArXiv e-prints [arXiv:1403.5237]
Berg, D. A., Skillman, E. D., Marble, A. R., et al. 2012, ApJ, 754, 98
Bittner, A., Falcón-Barroso, J., Nedelchev, B., et al. 2019, A&A, 628, A117
Bonoli, S., Marín-Franch, A., Varela, J., et al. 2021, A&A, 653, A31
Boquien, M., Burgarella, D., Roehlly, Y., et al. 2019, A&A, 622, A103
Bournaud, F. 2010, ASP Conf. Ser., 423, 177
Bournaud, F., & Duc, P.-A. 2006, A&A, 456, 481
Bournaud, F., Chapon, D., Teyssier, R., et al. 2011, ApJ, 730, 4
Bruzual, G., & Charlot, S. 2003, MNRAS, 344, 1000
Calzetti, D., Armus, L., Bohlin, R. C., et al. 2000, ApJ, 533, 682
Cannon, J. M., Martinkus, C. P., Leisman, L., et al. 2015, AJ, 149, 72
Cappellari, M. 2017, MNRAS, 466, 798
Casas, R. A., Arias, V., Peña Ramírez, K., & Kroupa, P. 2012, MNRAS, 424, 1941
Cautun, M., Bose, S., Frenk, C. S., et al. 2015, MNRAS, 452, 3838
Chabrier, G. 2003, PASP, 115, 763
Collins, M. L. M., Martin, N. F., Rich, R. M., et al. 2015, ApJ, 799, 13
Croxall, K. V., van Zee, L., Lee, H., et al. 2009, ApJ, 705, 723
Dabringhausen, J., & Kroupa, P. 2013, MNRAS, 429, 1858
Delgado-Donate, E. J., Muñoz-Tuñón, C., Deeg, H. J., et al. 2003, A&A, 402, 921
Dey, A., Schlegel, D., Lang, D., et al. 2019, AJ, 157, 168
Dobbs, C. L., Theis, C., Pringle, J. E., & Bate, M. R. 2010, MNRAS, 403, 625
Draine, B. T., Aniano, G., Krause, O., et al. 2014, ApJ, 780, 172
Du, L., Du, W., Cheng, C., et al. 2024, ApJ, 964, 85
Duarte Puertas, S., Vilchez, J. M., Iglesias-Páramo, J., et al. 2022, A&A, 666, A186
Duc, P.-A. 2012, Astrophys. Space Sci. Proc., 305
Duc, P.-A., & Mirabel, I. F. 1994, A&A, 289, 83
Duc, P.-A., Brinks, E., Wink, J. E., & Mirabel, I. F. 1997, A&A, 326, 537
Duc, P.-A., Brinks, E., Springel, V., et al. 2000, AJ, 120, 1238
Duc, P.-A., Bournaud, F., & Masset, F. 2004, A&A, 427, 803
Duc, P.-A., Paudel, S., McDermid, R. M., et al. 2014, MNRAS, 440, 1458
Dumont, A., & Martel, H. 2021, MNRAS, 503, 2866
Eigenthaler, P., Ploeckinger, S., Verdugo, M., & Ziegler, B. 2015, MNRAS, 451, 2793
Eigenthaler, P., Puzia, T. H., Taylor, M. A., et al. 2018, ApJ, 855, 142
Ferrara, A., & Tolstoy, E. 2000, MNRAS, 313, 291
Flores, H., Hammer, F., Fouquet, S., et al. 2016, MNRAS, 457, L14
Fouquet, S., Hammer, F., Yang, Y., et al. 2012, MNRAS, 427, 1769
Gray, L. M., Rhode, K. L., Leisman, L., et al. 2023, AJ, 165, 197
Gnedin, N. Y., & Kravtsov, A. V. 2010, ApJ, 714, 287
Guo, Q., Hu, H., Zheng, Z., et al. 2020, Nat. Astron., 4, 246
Hammer, F., Yang, Y., Fouquet, S., et al. 2013, MNRAS, 431, 3543
Hancock, M., Smith, B. J., Hancock, M., et al. 2007, AJ, 133, 676
Hancock, M., Smith, B. J., Hancock, M., et al. 2009, AJ, 137, 4643
Haslbauer, M., Dabringhausen, J., Kroupa, P., Javanmardi, B., & Banik, I. 2019, A&A, 626, A47
Hatziminaoglou, E., Pérez-Fournon, I., Polletta, M., et al. 2005, AJ, 129, 1198
Hibbard, J. E., & Mihos, J. C. 1995, AJ, 110, 140
Houck, J. R., Charmandaris, V., Brandl, B. R., et al. 2004, ApJS, 154, 211
Hunsberger, S. D., Charlton, J. C., Zaritsky, D., et al. 1996, ApJ, 462, 50
Hunt, L. K., Thuan, T. X., Izotov, Y. I., & Sauvage, M. 2010, ApJ, 712, 164
Hunter, D. A., Hunsberger, S. D., & Roye, E. W. 2000, ApJ, 542, 137
Jackson, R. A., Kaviraj, S., Martin, G., et al. 2021, MNRAS, 502, 1785
Kaviraj, S., Darg, D., Lintott, C., et al. 2012, MNRAS, 419, 70
Kennicutt, R. C., & Evans, N. J. 2012, ARA&A, 50, 531
Kirby, E. N., Cohen, J. G., Guhathakurta, P., et al. 2013, ApJ, 779, 102
Lange, R., Moffett, A. J., Driver, S. P., et al. 2016, MNRAS, 462, 1470
Lee-Waddell, K., Spekkens, K., Chandra, P., et al. 2016, MNRAS, 460, 2945
Leitherer, C., Li, I.-H., Calzetti, D., et al. 2002, ApJS, 140, 303
Lelli, F., Duc, P.-A., Brinks, E., et al. 2015, A&A, 584, A113
Lelli, F., McGaugh, S. S., Schombert, J. M., et al. 2019, MNRAS, 484, 3267
Lilly, S. J., Carollo, C. M., Pipino, A., et al. 2013, ApJ, 772, 119
Lynden-Bell, D. 1976, MNRAS, 174, 695
Madden, S. C., Galliano, F., Jones, A. P., & Sauvage, M. 2006, A&A, 446, 877
Marcelin, M., Lecoarer, E., Boulesteix, J., Georgelin, Y., & Monnet, G. 1987, A&A, 179, 101
McConnachie, A. W. 2012, AJ, 144, 4
McGaugh, S. S. 2005, ApJ, 632, 859
McGaugh, S. S., Schombert, J. M., Bothun, G. D., et al. 2000, ApJ, 533, L99
Metz, M., & Kroupa, P. 2007, MNRAS, 376, 387
Mihos, J., Harding, P., Feldmeier, J., et al. 2005, ApJ, 631, 41
Miralles-Caballero, D., Colina, L., & Arribas, S. 2012, A&A, 538, 61
Montes, M., Trujillo, I., Karunakaran, A., et al. 2024, A&A, 681, A15
Okazaki, T., & Taniguchi, Y. 2000, ApJ, 543, 149
Osterbrock, D. E. 1989, Astrophysics of Gaseous Nebulae and Active Galactic Nuclei (University Science Books)
Pawlowski, M. S. 2018, MPLA, 33, 06
Pawlowski, M. S., Pflamm-Altenburg, J., & Kroupa, P. 2012, MNRAS, 423, 1109
Pérez-Montero, E. 2017, PASP, 129, 043001
Pham, K., Kravtsov, A., & Manwadkar, V. 2023, MNRAS, 520, 3937
Pilyugin, L. S., & Grebel, E. K. 2016, MNRAS, 457, 3678
Ploeckinger, S., Recchi, S., Hensler, G., & Kroupa, P. 2015, MNRAS, 447, 2512
Ploeckinger, S., Sharma, K., Schaye, J., et al. 2018, MNRAS, 474, 580
Recchi, S., & Hensler, G. 2007, A&A, 476, 841
Recchi, S., & Hensler, G. 2013, A&A, 551, 41
Recchi, S., Kroupa, P., & Ploeckinger, S. 2015, MNRAS, 450, 2367
Román, J., Jones, M. G., Montes, M., et al. 2021, A&A, 649, L14
Rosenberg, J. L., Wu, Y., Le Floc'h, E., et al. 2008, ApJ, 674, 814
Russell, S. C., & Dopita, M. A. 1992, ApJ, 384, 508
Samuel, J., Wetzel, A., Chapman, S., et al. 2021, MNRAS, 504, 1379
Sawala, T., Cautun, M., Frenk, C., et al. 2023, Nat. Astron., 7, 481
Sengupta, C., Dwarakanath, K. S., & Saikia, D. J. 2009, MNRAS, 397, 5
Sengupta, C., Saikia, D. J., & Dwarakanath, K. S. 2012, MNRAS, 420, 2
Sengupta, C., Scott, T. C., Paudel, S., et al. 2015, A&A, 584, 114
Silk, J., & Mamon, G. A. 2012, RAA, 12, 917
Smith, B. J., & Hancock, M. 2009, AJ, 138, 130
Smith, B. J., & Struck, C. 2010, AJ, 140, 1975
Smith, B. J., Struck, C., Appleton, P. N., et al. 2005, AJ, 130, 2117
Smith, B. J., Struck, C., Hancock, M., et al. 2007, AJ, 133, 791
Smith, B. J., Struck, C., Hancock, M., et al. 2008, AJ, 135, 2406
Smith, B. J., Giroux, M. L., Struck, C., et al. 2010, AJ, 139, 1212
Smith, R., Duc, P. A., Candlish, G. N., et al. 2013, MNRAS, 436, 839
Smith, B. J., Soria, R., Struck, C., et al. 2014, AJ, 147, 60
Smith, B. J., Zaragoza-Cardiel, J., Struck, C., et al. 2016, AJ, 151, 63
Sweet, S. M., Drinkwater, M. J., Meurer, G., et al. 2014, ApJ, 782, 35
Vazdekis, A., Sánchez-Blázquez, P., Falcón-Barroso, J., et al. 2010, MNRAS, 404, 1639
Weilbacher, P. M., Duc, P.-A., & Fritze-v. Alvensleben, U., 2003, A&A, 397, 545
Wen, Z.-Z., Zheng, X.-Z., Zhao, Y.-H., & Gao, Y. 2012, Ap&SS, 337, 729
Wetzstein, M., Naab, T., & Burkert, A. 2007, MNRAS, 375, 805
Whitney, B. A., Indebetouw, R., Babler, B. L., et al. 2004, ApJS, 154, 315
Yang, Y., Hammer, F., Fouquet, S., et al. 2014, MNRAS, 442, 2419
Zaragoza-Cardiel, J., Smith, B. J., Rosado, M., et al. 2018, ApJS, 234, 34S
Zaragoza-Cardiel, J., Fritz, J., Aretxaga, I., et al. 2019, MNRAS, 487, L61
Zaragoza-Cardiel, J., Fritz, J., Aretxaga, I., et al. 2020, MNRAS, 499, 1172
Zasov, A. V., Saburova, A. S., Egorov, O. V., et al. 2020, MNRAS, 498, 101
Zhou, Z.-M., Wu, H., Huang, L., et al. 2014, RAA, 14, 1393
Zwicky, F. 1956, Ergebnisse der exakten Naturwissenschaften, 29, 344